were taken at each visit from participants who received regular follow-up examinations.

The study protocol was approved by the ethical review board of Nagasaki University and of the other hospitals involved. All women were informed of the purpose of the study and gave their consent.

HPV genotyping test

Genotyping of HPV DNA in the SurePath preservative fluid was performed using the Linear Array HPV Genotyping Test kit (Roche Diagnostics, Indianapolis, IN, USA). The kit uses PGMY09/PGMY11 primers[7] to amplify the L1 conserved region. Following PCR amplification, hybridization of the HPV amplicon was performed using an array of oligonucleotide probes that allowed independent identification of individual HPV genotypes. This kit can detect 37 HPV genotypes (6, 11, 16, 18, 26, 31, 33, 35, 39, 40, 42, 45, 51, 52, 53, 54, 55, 56, 58, 59, 61, 62, 64, 66, 67, 68, 69, 70, 71, 72, 73 (MM9), 81, 82 (MM4), 83 (MM7), 84 (MM8), IS39 and CP6108 (89)). For consistency with previous studies, we considered 16 HPV genotypes (16, 18, 31, 33, 35, 45, 51, 52, 53, 56, 58, 59, 66, 68, 73 and 82) as high-risk genotypes that are related to cervical cancer.[8–10]

RESULTS

A total of 151 women were enrolled in the study. In all, 79 women were in the first trimester of their pregnancy, 18 were in the second trimester, 51 were in the third trimester and 3 were postpartum. Fifty-four women (35.8%; 54/151), with an average age of 30, were positive for HPV on their first hospital visit. Forty-nine women (32.5%; 49/151) were infected by at least one high-risk HPV and five women were infected by only low-risk HPV. The three most prevalent high-risk HPV genotypes were HPV 52 (31.5%; 17/54), HPV 16 (29.6%; 16/51) and HPV 31 (13.0%; 7/51) (Table 1). The HPV infection pattern (negative, single infection and multiple infection) was significantly different depending on the trimester of the pregnancy (χ^2-test; $P<0.01$ (Pearson)).

Table 1 Prevalence of HPV infection in pregnant Japanese women

	Trimester			
	1st	*2nd*	*3rd*	*Total (%)*[a]
n	79	18	51	148
HPV negative	48	7	39	94
Single infection	17	9	10	36 (66.7)
Multiple infection	14	2	2	18 (33.3)
HPV type				
(high-risk type)				
16	7	6	3	16 (29.6)
18	2	2	1	5 (9.3)
31	5	0	2	7 (13.0)
33	3	0	0	3 (5.6)
51	2	0	0	2 (3.7)
52	14	2	1	17 (31.5)
53	1	0	0	1 (1.9)
56	3	0	0	3 (5.6)
58	2	1	2	5 (9.3)
68	2	0	0	2 (3.7)
82	1	0	1	2 (3.7)
(Low-risk type)				
6	2	1	0	3 (5.6)
39	1	0	1	2 (3.7)
42	0	0	1	1 (1.9)
54	1	1	0	2 (3.7)
61	3	0	1	4 (7.4)
71	0	0	1	1 (1.9)
84	0	0	2	2 (3.7)
CP6108 (89)	2	0	0	2 (3.7)

Abbreviation: HPV, human papillomavirus.
[a]The denominator was the number of HPV-positive women.

DISCUSSION

The influence of pregnancy on the natural course of HPV infection is not understood. Several reports show that the prevalence of HPV infection in pregnant women is variable at 10–60%, depending on age, region and HPV detection methods.[11–14] The HPV infection rate in pregnant women in this report was 35%. There are few reports of HPV infection rates in pregnant Japanese women. One report by Takakuwa *et al.*[15] showed the prevalence of HPV in pregnant Japanese women to be 12.5%. The difference between this report and our results may be because of the detection method used, PCR-reverse hybridization (our study) and PCR-restriction fragment length polymorphism (Takakuwa *et al.*), and the number of detectable HPV genotypes.

Several other studies[16,17] show the clearance of HPV infection may accelerate in the third trimester and postpartum. In our study, the HPV infection pattern differed significantly according to the pregnancy trimester. In particular, in the first trimester, multiple HPV infection was observed more often than in the later periods. This observation may be explained by changes in sexual behavior and/or by immunological factors. Pregnant women tend to be less sexually active and their immune response against HPV is reduced. The accelerated clearance of HPV may be due to the host immune system normalizing during the third trimester.[18]

Our results showed that HPV 16 and HPV 52 were the two most common genotypes among pregnant Japanese women. Our data among 154 non-pregnant Japanese women also showed that HPV 16 and HPV 52 were the two most common genotype. The prevalence of HPV genotype in Japanese pregnant women may not show pregnant-specific features. Other reports using HPV genotyping tests also showed that HPV 52 was a more common genotype among Japanese individuals who had either normal cytology or cervical neoplastic lesions compared with individuals in other countries.[10,19,20]

In Japan, a commercial cervical cancer vaccine finally became available after December 2009. This study has some limitations because we obtained data from pregnant women; however, our data from pre-vaccination women on the distribution of genital HPV infections in the region where HPV 52 is more prevalent are important for the understanding of the cross-reactivity of a bivalent HPV vaccine.[17,21]

ACKNOWLEDGEMENTS

K Yamasaki was supported by the Nagasaki University President's Fund Grant. K Miura, S Miura and H Masuzaki were supported by a Grant-in-Aid for Young Scientists (B) (No. 21791567, No. 22791535) and for Scientific Research (C) (No. 22591827) from the Ministry of Education, Culture, Sports, Science and Technology of Japan. K Miura was was supported by The Grant of National Center for Child Health and Development (20C-1), Japan. K Yoshiura was supported by Grants-in-Aid for Scientific Research from the Ministry of Health, Labour and Welfare, Japan.

1 Shimada, T., Miyashita, M., Miura, S., Nakayama, D., Miura, K., Fukuda, M. *et al.* Genital human papilloma virus infection in mentally-institutionalized virgins. *Gynecol. Oncol.* **106,** 488–489 (2007).
2 Moscicki, A. B., Palefsky, J., Smith, G., Siboshski, S. & Schoolnik, G. Variability of human papillomavirus DNA testing in a longitudinal cohort of young women. *Obstet. Gynecol.* **82**(Part 1), 578–585 (1993).
3 Woodman, C. B., Collins, S., Winter, H., Bailey, A., Ellis, J., Prior, P. *et al.* Natural history of cervical human papillomavirus infection in young women: a longitudinal cohort study. *Lancet.* **357,** 1831–1836 (2001).
4 Ho, G. Y., Bierman, R., Beardsley, L., Chang, C. J. & Burk, R. D. Natural history of cervicovaginal papillomavirus infection in young women. *N. Engl. J. Med.* **338,** 423–428 (1998).
5 Sethi, S., Muller, M., Schneider, A., Blettner, M., Smith, E., Turek, L. *et al.* Serologic response to the E4, E6, and E7 proteins of human papillomavirus type 16 in pregnant women. *Am. J. Obstet. Gynecol.* **178,** 360–364 (1998).
6 Michelin, D., Gissmann, L., Street, D., Potkul, R. K., Fisher, S., Kaufmann, A. M. *et al.* Regulation of human papillomavirus type 18 *in vivo*: effects of estrogen and progesterone in transgenic mice. *Gynecol. Oncol.* **66,** 202–208 (1997).
7 Gravitt, P. E., Peyton, C. L., Alessi, T. Q., Wheeler, C. M., Coutlee, F., Hildesheim, A. *et al.* Improved amplification of genital human papillomaviruses. *J. Clin. Microbiol.* **38,** 357–361 (2000).
8 Walboomers, J. M., Jacobs, M. V., Manos, M. M., Bosch, F. X., Kummer, J. A., Shah, K. V. *et al.* Human papillomavirus is a necessary cause of invasive cervical cancer worldwide. *J. Pathol.* **189,** 12–19 (1999).
9 Munoz, N., Bosch, F. X., de Sanjose, S., Herrero, R., Castellsague, X., Shah, K. V. *et al.* Epidemiologic classification of human papillomavirus types associated with cervical cancer. *N. Engl. J. Med.* **348,** 518–527 (2003).
10 Asato, T., Maehama, T., Nagai, Y., Kanazawa, K., Uezato, H. & Kariya, K.-I.Alarge Case-control study of cervical cancer risk associated with human papillomavirus infection in Japan, by nucleotide sequencing-based genotyping. *J. Infect. Dis.* **189,** 1829–1832 (2004).
11 Kemp, E. A., Hakenewerth, A. M., Laurent, S. L., Gravitt, P. E. & Stoerker, J. Human papillomavirus prevalence in pregnancy. *Obstet. Gynecol.* **79,** 649–656 (1992).
12 Banura, C., Franceschi, S., van Doorn, L. J., Arslan, A., Kleter, B., Wabwire-Mangen, F. *et al.* Prevalence, incidence and clearance of human papillomavirus infection among young primiparous pregnant women in Kampala, Uganda. *Int. J. Cancer.* **123,** 2180–2187 (2008).
13 Chan, P. K., Chang, A. R., Tam, W. H., Cheung, J. L. & Cheng, A. F Prevalence and genotype distribution of cervical human papillomavirus infection: comparison between pregnant women and non-pregnant controls. *J. Med. Virol.* **67,** 583–588 (2002).
14 Morrison, E. A., Gammon, M. D., Goldberg, G. L., Vermund, S. H. & Burk, R. D. Pregnancy and cervical infection with human papillomaviruses. *Int. J. Gynaecol. Obstet.* **54,** 125–130 (1996).
15 Takakuwa, K., Mitsui, T., Iwashita, M., Kobayashi, I., Suzuki, A., Oda, T. *et al.* Studies on the prevalence of human papillomavirus in pregnant women in Japan. *J. Perinat. Med.* **34,** 77–79 (2006).
16 Fife, K. H., Katz, B. P., Brizendine, E. J. & Brown, D. R. Cervical human papillomavirus deoxyribonucleic acid persists throughout pregnancy and decreases in the postpartum period. *Am. J. Obstet. Gynecol.* **180,** 1110–1114 (1999).
17 Rando, R. F., Lindheim, S., Hasty, L., Sedlacek, T. V., Woodland, M. & Eder, C. Increased frequency of detection of human papillomavirus deoxyribonucleic acid in exfoliated cervical cells during pregnancy. *Am. J. Obstet. Gynecol.* **161,** 50–55 (1989).
18 Nobbenhuis, M. A., Helmerhorst, T. J., van den Brule, A. J., Rozendaal, L., Bezemer, P. D., Voorhorst, F. J. *et al.* High-risk human papillomavirus clearance in pregnant women: trends for lower clearance during pregnancy with a catch-up postpartum. *Br. J. Cancer.* **87,** 75–80 (2002).
19 Miura, S., Matsumoto, K., Oki, A., Satoh, T., Tsunoda, H., Yasugi, T. *et al.* Do we need a different strategy for HPV screening and vaccination in East Asia? *Int. J. Cancer.* **119,** 2713–2715 (2006).
20 Inoue, M., Sakaguchi, J., Sasagawa, T. & Tango, M. The evaluation of human papillomavirus DNA testing in primary screening for cervical lesions in a large Japanese population. *Int. J. Gynecol. Cancer.* **16,** 1007–1013 (2006).
21 Paavonen, J., Naud, P., Salmeron, J., Wheeler, C. M., Chow, S. N., Apter, D. *et al.* Efficacy of human papillomavirus (HPV)-16/18 AS04-adjuvanted vaccine against cervical infection and precancer caused by oncogenic HPV types (PATRICIA): final analysis of a double-blind, randomised study in young women. *Lancet.* **374,** 301–314 (2009).

OPEN ACCESS Freely available online

PLoS one

Identification of Novel Schizophrenia Loci by Homozygosity Mapping Using DNA Microarray Analysis

Naohiro Kurotaki[1]*, Shinya Tasaki[1], Hiroyuki Mishima[2,3], Shinji Ono[1], Akira Imamura[1], Taeko Kikuchi[1], Nao Nishida[4], Katsushi Tokunaga[4], Koh-ichiro Yoshiura[2], Hiroki Ozawa[1]

1 Department of Neuropsychiatry, Nagasaki University Graduate School of Biomedical Sciences, Nagasaki, Japan, **2** Department of Human Genetics, Nagasaki University Graduate School of Biomedical Sciences, Nagasaki, Japan, **3** Nagasaki University Global Center of Excellence Program, Nagasaki, Japan, **4** Department of Human Genetics, Graduate School of Medicine, The University of Tokyo, Tokyo, Japan

Abstract

The recent development of high-resolution DNA microarrays, in which hundreds of thousands of single nucleotide polymorphisms (SNPs) are genotyped, enables the rapid identification of susceptibility genes for complex diseases. Clusters of these SNPs may show runs of homozygosity (ROHs) that can be analyzed for association with disease. An analysis of patients whose parents were first cousins enables the search for autozygous segments in their offspring. Here, using the Affymetrix® Genome-Wide Human SNP Array 5.0 to determine ROHs, we genotyped 9 individuals with schizophrenia (SCZ) whose parents were first cousins. We identified overlapping ROHs on chromosomes 1, 3, 4, 5, 6, 7, 8, 9, 10, 11, 12, 13, 16, 17, 19, 20, and 21 in at least 3 individuals. Only the locus on chromosome 5 has been reported previously. The ROHs on chromosome 5q23.3–q31.1 include the candidate genes histidine triad nucleotide binding protein 1 (*HINT1*) and acyl-CoA synthetase long-chain family member 6 (*ACSL6*). Other overlapping ROHs may contain novel rare recessive variants that affect SCZ specifically in our samples, given the highly heterozygous nature of SCZ. Analysis of patients whose parents are first cousins may provide new insights for the genetic analysis of psychiatric diseases.

Citation: Kurotaki N, Tasaki S, Mishima H, Ono S, Imamura A, et al. (2011) Identification of Novel Schizophrenia Loci by Homozygosity Mapping Using DNA Microarray Analysis. PLoS ONE 6(5): e20589. doi:10.1371/journal.pone.0020589

Editor: Xiang Yang Zhang, Baylor College of Medicine, United States of America

Received November 28, 2010; **Accepted** May 6, 2011; **Published** May 31, 2011

Funding: NK was supported in part by grants from Grant-in-Aid for Scientific Research (No. 19591363) and by grants from the Mitsubishi Pharma Research Foundation. KY was supported in part by Grant-in-Aid for Scientific Research from the Ministry of Health, Labor, and Welfare, from the Takeda Scientific Foundation, and from the Naito Foundation. This work was also supported by Nagasaki University Global COE program, global strategic center for radiation health risk control. The funders had no role in study design, data collection and analysis, decision to publish, or preparation of the manuscript.

Competing Interests: The authors have declared that no competing interests exist.

* E-mail: naokuro@nagasaki-u.ac.jp

Introduction

Schizophrenia (SCZ) is categorized as a severe chronic debilitating psychosis that affects approximately 1% of the global population. Although genetic factors are reported to contribute to the disease and multiple responsible loci have been identified from linkage analysis and case-control association studies, there have been few reproducible results to date [1].

Morrow et al. (2008) [2] suggested that homozygosity mapping is a powerful tool not only for investigating single gene defects but also for rare genomic variants in complex traits. They observed homozygous deletions in patients with autistic disorders and concluded that genomic alterations might be a subset of disease-causing mutations in chromosomal regions. The increased susceptibility to SCZ observed in consanguineous families suggests that genomic recessive variations may be involved in its etiology. [3–5] Considering this and other results, we hypothesized that homozygosity mapping, including identical by descent (IBD) analysis, would be a highly constructive method for identifying the loci responsible for SCZ.

We hypothesized that runs of homozygosity (ROHs) could contribute to SCZ by a recessive effect. We use the term "ROH" [6] instead of loss of heterozygosity (LOH) for regions where homozygous genotypes are contiguous because LOH implies heterozygous deletions or hemizygosity, while ROH suggests consecutive homozygous regions. Recessive effects are obtained by genetic variations including single nucleotide variations, small insertions/deletions, structural variations, and chromosomal rearrangements. These variations may affect amino acid sequences or the control of gene expression, including small RNA expression.

Here, we describe a homozygosity mapping strategy that consisted of 2 stages (Figure 1). The first stage aimed to find the appropriate size threshold for autosomal ROHs that would distinguish ROHs specifically existing in the offspring of first-cousin marriages from those that commonly exist in the offspring of non-consanguineous marriages. By comparing the size distribution of ROHs between the offspring of first-cousin marriages and non-consanguineous marriages, we concluded that ROHs >2.1 Mb in size in the offspring of consanguineous marriages can be assumed to be IBD segments from an individual 3 generations before. The second stage aimed to find shared ROHs among patient with SCZ using 2 models. In Model I, an autosomal ROH size threshold was applied to filter out smaller ROHs. Larger ROHs were assessed to find overlaps among the patients. In Model II, after filtering by the ROH size threshold, ROHs shared by the siblings of patients and ROHs of other patients were assessed to find overlaps. The overlapping ROHs we identified potentially contain SCZ causative regions that are specific to our samples because of the heterogeneous nature of SCZ.

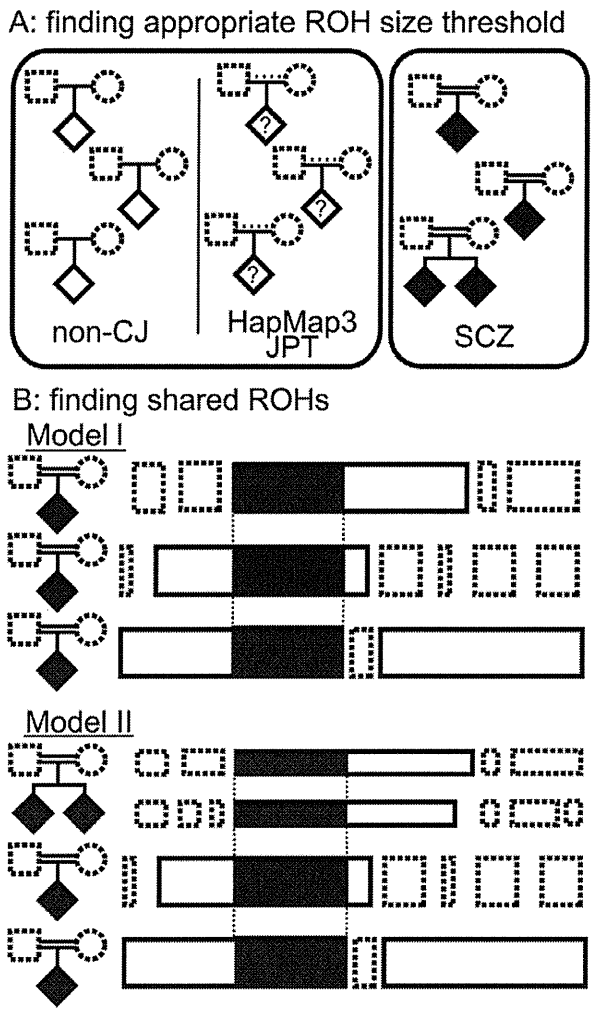

Figure 1. Two-stage design of this study. A, the first stage was to find an appropriate autosomal run of homozygosity (ROH) size threshold to distinguish specific ROHs from the offspring of first-cousin marriages from ROHs in the offspring of non-consanguineous marriages. The size distribution of ROHs in our non-consanguineous Japanese (non-CJ) and schizophrenia (SCZ) samples was compared. Non-CJ samples are the offspring of non-consanguineous marriages that were validated by interview. Here, SCZ samples were used as the offspring of first-cousin marriages regardless of phenotype. Samples from parents were not used in this study (dashed squares and circles). To confirm our strategy, we also assessed HapMap3 JPT samples, which do not have information for phenotypes or family consanguinity (dashed and solid lines between parents). B, the second stage was to find shared ROHs among the SCZ samples as patients with schizophrenia. In Model I, an autosomal ROH size threshold was applied to filter out smaller ROHs (dashed open boxes). Larger ROHs (solid open boxes) were assessed to find overlaps among patients (solid boxes). In Model II, after filtering by the ROH size threshold, ROHs shared by the siblings of patients and ROHs of other patients were assessed to find overlaps. In this study, the gender of the samples was not matched (diamonds) because we only evaluated autosomal ROHs.
doi:10.1371/journal.pone.0020589.g001

Materials and Methods

1. Samples

A total of 9 subjects with SCZ (3 males and 6 females, aged 31–56 years) (SCZ individuals) were recruited to this study after being diagnosed as having typical paranoid schizophrenia by a certified psychiatrist (N.K.) using the *Diagnostic and Statistical Manual of Mental Disorders*, Fourth Edition, Text Revision (DSM-IV-TR) and the *Structured Clinical Interview for DSM-IV Axis I Disorders* (SCID). The study received ethics approval from the Committee for Ethical Issues on Human Genome and Gene Analysis at Nagasaki University, Japan. All of the patients were from the main islands of Japan, excluding Okinawa. We obtained written informed consent from all participants. The consanguineous patients were from 8 first-cousin marriages. Seven individuals (patients a to g) were unrelated and 2 were siblings (patients h-1 and h-2). We also recruited 92 healthy individuals from non-consanguineous marriages (non-CJ individuals) from the main islands of Japan, excluding Okinawa. We confirmed consanguinity by interview. We did not match for gender in the SCZ and non-CJ individuals because we only intended to analyze autosomal chromosomes.

After obtaining written informed consent, genomic DNA was isolated from peripheral blood. We did not collect blood samples from the patients' parents, except for 1 patient, or siblings; however, we confirmed that they had no history of psychiatric illness, with the exception of the older brother of patient g, by direct interview or from the medical records of the other related individuals.

Furthermore, we also assessed the International HapMap Project [7] phase 3 data of the Japanese in Tokyo (HapMap3 JPT) to evaluate the non-CJ individuals. Raw signal intensity files (CEL files) obtained using Affymetrix Genome-Wide Human SNP Array 6.0 (Affy6.0) were downloaded from http://www.hapmap.org/.

2. Microarray analysis

We performed genome-wide SNP genotyping of 9 SCZ samples and 92 non-CJ samples using the Affymetrix Genome-Wide Human SNP Array 5.0 (Affy5.0) according to the manufacturer's instructions. Our microarray data is MIAME compliant and the raw data has been deposited in the CIBEX database (CIBEX accession number: CBX141).

3. ROH detection

We generated the CHP genotype files from the CEL signal intensity files using the BRLMM-P genotype calling program [8,9]. For the detection of ROHs, we analyzed the CHP files with a hidden Markov model (HMM)-based ROH detection function of the Partek® Genomics Suite (Partek GS) software version 6.5 build 6.11.0207 (Partek, St. Louis, MO, USA). We applied the following default HMM parameters: max probability = 0.99, genomic decay = 0 (disabled), genotype error = 0.01, and default frequency = 0.3. We did not adopt the baseline files.

Detected ROHs were statistically analyzed and visualized (Figures 2 and 3; Tables 1 and 2) by using in-house scripts written in the R language [10]. The optimization of histogram bandwidths and the estimation of the probability density distributions were performed using the "KernSmooth" package of R [11].

Furthermore, to validate the data quality of our non-CJ samples, we also compared our data to HapMap3 JPT. Affy6.0 raw signal intensity data in CEL files were subjected to allele calling using Birdseed software version 2 [12]. SNP genotypes of shared loci between Affy6.0 and Affy5.0 were extracted and processed as well as the non-CJ and SCZ datasets to detect ROHs.

4. Detection of potential genetic loci for SCZ by overlapping ROHs

To detect the overlapping ROHs among the SCZ dataset, the identified ROHs were filtered by a size threshold on Partek GS,

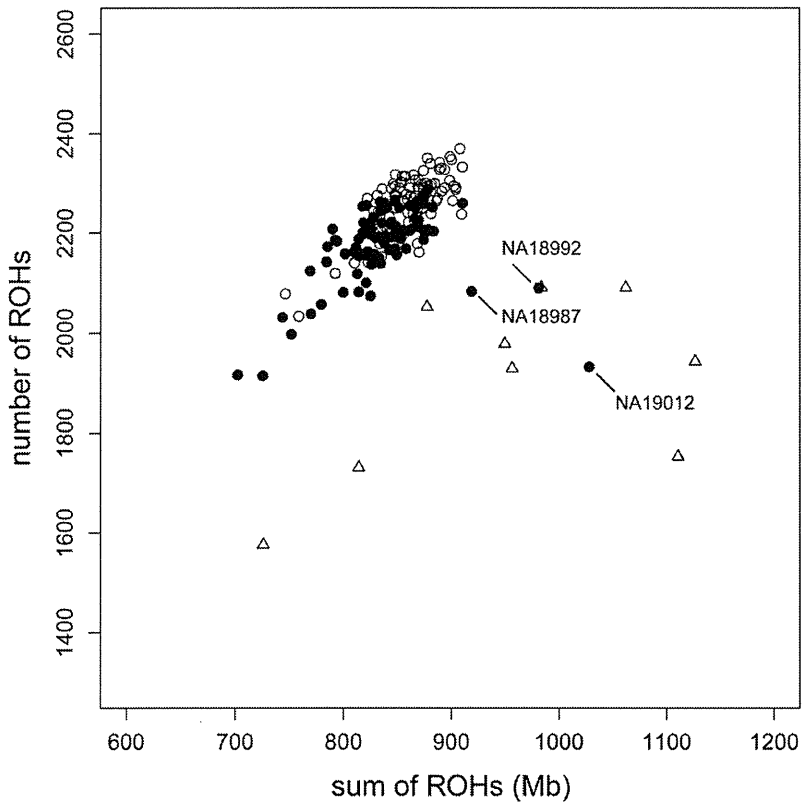

Figure 2. Distribution of the size and number of individual autosomal runs of homozygosity (ROHs). Sums and total numbers of individual ROHs are shown by circles and triangles indicating unrelated Japanese individuals (non-CJ: 92 samples) and the offspring of first-cousin marriages with schizophrenia (SCZ: 9 samples), respectively.
doi:10.1371/journal.pone.0020589.g002

analyzed using an in-house Ruby script (available on request) to generate a table of overlapping ROHs, and visualized with Partek GS. Then, we extracted the loci shared among more than 3 unrelated individuals (Model I) (Table S1). Furthermore, on the basis of the hypothesis that concordant sibling cases share causal loci, we detected the loci shared among 2 sibling cases (h-1 and h-2) (Model II) and found the ROHs that were shared by 1 or more of the unrelated samples (Table 3).

Results

1. Determination of the ROH size threshold discriminating the offspring from non-consanguineous and first-cousin marriages

We genotyped 440 794 SNPs in each individual. Genotype calling rates for each sample ranged from 97.23–98.83% and their call rates were high and accurate enough for their subsequent evaluation. We utilized the data from 92 non-CJ and 91 HapMap3 JPT samples in addition to the data from 9 SCZ individuals.

Our homozygosity mapping strategy utilized differences in the length distribution of ROHs between offspring from consanguineous and non-consanguineous marriages. Individuals from consanguineous families are expected to have an increased number of longer ROHs containing autozygous segments. These segments were also expected to be discriminated by their length from ROHs containing homozygous segments by chance or by linkage disequilibrium (LD). To demonstrate the strategy, we performed detailed comparisons of the length distribution of ROHs between the non-CJ, HapMap3 JPT, and SCZ datasets.

We initially plotted the total number and size of ROHs in the non-CJ, HapMap3 JPT, and SCZ datasets (Figure 2). The non-CJ and HapMap3 JPT datasets clustered together, except for 3 individuals in HapMap JPT. These 3 outlier individuals, NA18987, NA18992 [13], and NA19012 [14], have been assumed to be from consanguineous families; indeed, the distribution of these samples was similar to that of our offspring from first-cousin marriages (Figure 2).

We then analyzed the length distribution of ROHs in the non-CJ and SCZ datasets. Bar plot histograms of the length of ROHs were obtained and the probability density curves were estimated by the "KernSmooth" package in R (Figure 3A–D). Descriptive statistics of these plots are also shown in Table 1. Both datasets produced bell curve-like distributions in the $\log_{10}$ scale on the x-axis to indicate the length of each ROH; however, the SCZ dataset showed a secondary peak in the larger ROH region. We expected that the autozygous region from the founders of the third ancestral generation (great-grandparents) would be larger in the SCZ dataset than in the non-CJ dataset, in whom LD may encompass ROHs by chance. The proportion of larger ROHs in the SCZ dataset was clearly higher than in the non-CJ dataset. As we can expect that 1/16 of the whole genome in the offspring of first-cousin marriages would be autozygous regions from their great-grandparents, we highlighted the graphs in Figure 3B and

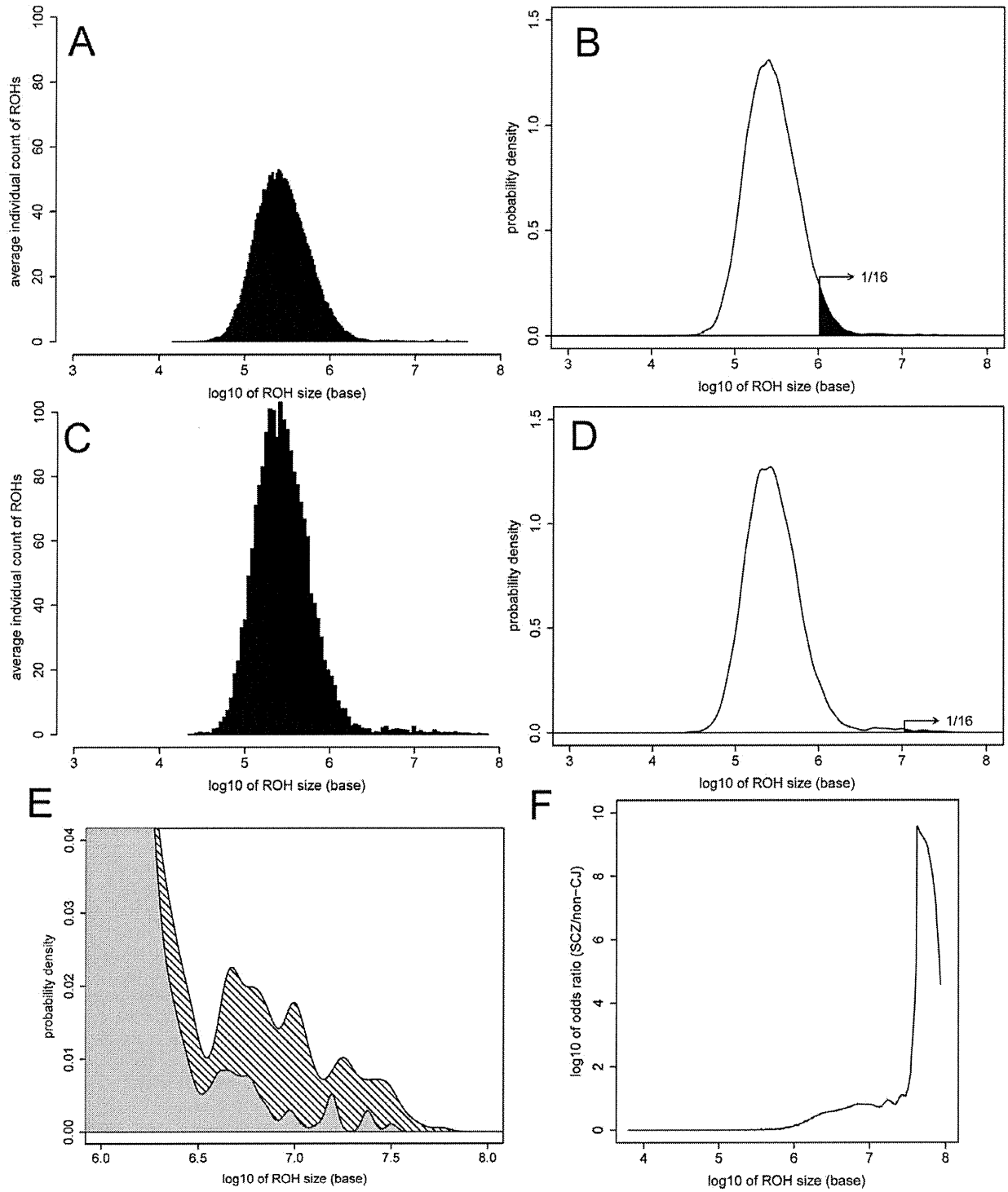

Figure 3. Size distribution of autosomal runs of homozygosity (ROHs). In the size distribution plot of non-consanguineous Japanese (non-CJ; A and B) and schizophrenia (SCZ; C and D) samples, the x-axis indicates the ROH size (log_{10} scale). A and C, individual average frequency of the ROHs as histograms. B and D, estimated probability density corresponding to each histogram. Black areas shows 1/16 (6.25%) of autosomes, which is equivalent to the expected sum of autozygous regions in the offspring of a first-cousin marriage. E, enlarged overlap of B (gray) and D (hatched). F, SCZ/non-CJ odds ratio plot. X-axis indicates the size of the ROHs (log_{10} scale). Y-axis (log_{10} scale) indicates the ratio of areas exceeding the given ROH size threshold in the estimated probability distributions of the SCZ and non-CJ datasets.
doi:10.1371/journal.pone.0020589.g003

Table 1. Autosomal runs of homozygosity (ROHs) size distribution, where descriptive statistics of ROH sizes were detected with Partek GS.

Dataset	N	Minimum[a]	Mode[b]	Maximum[c]	Average sum[d]
HM3JPT[e]	88	19 750 (14)	256 499 (27)	32 000 000 (1252)	831 159 144
non-CJ[f]	92	18 160 (14)	248 288 (27)	32 250 000 (1921)	859 784 793
SCZ[g]	9	27 380 (14)	258 488 (38)	57 810 000 (9896)	956 266 858

[a]Minimum ROH size in all individuals from each dataset.
[b]Mode ROH size in all individuals from each dataset.
[c]Maximum ROH size in all individuals from each dataset.
[d]Average sum is the average total ROH size per individual from each dataset.
[e]The International HapMap Project phase 3 Japanese in Tokyo. Three samples, NA18987, NA18992, and NA19012, of 91 samples are omitted because they are potentially the offspring of a consanguineous marriage.
[f]Non-consanguineous Japanese.
[g]Schizophrenia.
Numbers are in bases, and the numbers in parentheses are the included probe sets.
doi:10.1371/journal.pone.0020589.t001

3D at the point where the total sum of length in the upper tail of the ROH distribution reaches 179.2 Mb, which is 1/16 of the 2 867 732 772 bases total size of the autosomal haploid genome, according to the statistics from the NCBI Build 36.1 assembly (2006) [16]. This analysis suggested that it is highly probable that the longer ROHs would be inherited from the great-grandparents; however, it should be mentioned that genomic regions with less recombination tend to have longer ROHs.

To show further differences in the probability density distribution of the SCZ and non-CJ individuals, we also plotted an SCZ/non-CJ odds ratio (OR) plot (Figure 3F and Table 2), which indicates the ratio of probability for the existence of ROHs in each dataset over a given threshold length. To determine the overlapping ROH regions shared among the SCZ dataset, we adopted OR = 3.0 and the corresponding threshold of 2 137 962 bases to ensure practical power and to detect smaller IBD regions by recombination.

2. Determination of potential SCZ genetic loci by overlapping ROHs

The sum lengths of the overlapping regions among 0–7 independent family patients are shown in Figure 4, and the calculated percentage sum length among a given number of patients and more in the autosomal genome were as follows: 100%, 51.7%, 13.6%, 6.0%, 1.9%, 1.3%, and 0.6%. Considering the statistics, we adopted a minimum of 3 patients for identifying candidate loci. Figure 5 shows a schema of the overlapping ROHs within autosomes and their positions are summarized in Table S1.

Overlapping ROHs found in 3 or more SCZ individuals on chromosomes 1, 3, 4, 5, 6, 7, 8, 9, 10, 11, 12, 13, 16, 17, 19, 20, and 21 (Figure 5A) suggested that many loci are potentially associated with SCZ in our patients. Only the locus on chromosome 5 has been reported in a previous linkage analysis of SCZ [16]. The ROHs were expanded by the analysis of 4 additional individuals; however, no additional loci were detected (data not shown). The locus on chromosome 5q23.3–q31.1 included the regions containing the histidine triad nucleotide binding protein 1 (*HINT1*) and acyl-CoA synthetase long-chain family member 6 (*ACSL6*) genes. Our results suggest that recessive variants of these candidate genes could be involved in the pathogenesis of SCZ in our patients.

In the analysis of 2 siblings (h-1 and h-2) from a first-cousin marriage, we searched for the ROH regions shared by the siblings as a single gene defect. The detection of loci shared by the siblings and 1 or more unrelated individuals demonstrated ROHs on chromosomes 1, 5, 7, 8, 10, 12, 13, 16, 17, 19, and 21 that might be causative for SCZ (Figure 5B). Those loci did not include any previously reported candidate genes. Interestingly, among the loci detected in Figure 5A and 5B, there were no overlapping loci identified in this study.

Table 2. Thresholds, individual average sums of runs of homozygosity (ROHs), its ratio in the autosomal genome, and the individual average encompassed number of ROHs corresponding to the odds ratios.

Odds ratio	Threshold (base)	Non-CJ[a] dataset			SCZ[b] dataset		
		sum (base)	Autosomal ratio (%)	# of ROHs	sum (base)	Autosomal ratio (%)	# of ROHs
1.3	1 000 000	185 411 092	6.5	93.2	420 200 807	14.7	123.6
2.0	1 548 817	110 468 918	3.9	30.6	341 258 405	11.9	52.7
00							
3.0	2 137 962	81 383 855	2.8	13.8	309 296 125	10.8	33.8
4.0	3 630 781	65 633 075	2.3	7.6	288 028 919	10.0	25.4
5.0	5 128 614	53 423 627	1.9	4.7	263 695 116	9.2	19.8
10.0	24 547 089	7 925 263	0.3	0.3	85 167 811	3.0	2.7

[a]Non-consanguineous Japanese.
[b]Schizophrenia.
doi:10.1371/journal.pone.0020589.t002

Table 3. Novel loci identified in this study that are different from those in Table S1, for the segments overlapping in more than 1 unrelated individual and the common regions between the 2 siblings (cases h-1 and h-2).

Chromosome	Start	End	Samples	# Samples[a]	Length	Cytoband
1	146258078	148749860	h-1, h-2, a	3	2491783	1q21.1-q21.2
5	45437574	49631829	h-1, h-2, d	3	4194256	5p12-q11.1
5	117360252	120214932	h-1, h-2, f	3	2854681	5q23.1
5	120214932	122586267	h-1, h-2, f, g	4	2371336	5q23.1-23.2
7	57594442	62282881	h-1, h-2, b, f	4	4688440	7p11.2-q11.21
8	129121122	131617749	h-1, h-2, b	3	2496628	8q24.21-q24.22
8	132434559	139244531	h-1, h-2, b	3	6809973	8q24.22-24.23
10	37363792	37599485	h-1, h-2, e	3	235694	10p11.21
10	37599485	37874740	h-1, h-2, e, g	4	275256	10p11.21
10	37874740	42217616	h-1, h-2, c, e, g	5	4342877	10p11.21-q11.21
12	33982292	36255461	h-1, h-2, a, d	4	2273170	12p11.1-q11
13	35366458	43580724	h-1, h-2, g	3	8214267	13q13.3-14.11
16	28924029	29606107	h-1, h-2, c	3	682079	16p11.2
16	29606107	29657036	h-1, h-2, c, f	4	50930	16p11.2
16	29657036	29680943	h-1, h-2, c, d, f	5	23908	16p11.2
16	29680943	31277953	h-1, h-2, b, c, d, f	6	1597011	16p11.2
16	34467305	34647935	h-1, h-2, a, b, c, d, f, g	8	180631	16p11.1
16	34647935	45122807	h-1, h-2, a, c, d, f, g	7	10474873	16p11.1-q11.2
16	45122807	47094922	h-1, h-2, a, b, c, d, f, g	8	1972116	16q11.2-q12.1
17	29659797	32811528	h-1, h-2, a	3	3151732	17q12
19	37676724	40349191	h-1, h-2, a	3	2672468	19q13.11-13.12
21	19821557	20188026	h-1, h-2, g	3	366470	21q21.2

[a]Number of individuals (including h-1 and h-2) who shared the region; for example, 5 indicates that 3 other individuals shared the common region of the 2 siblings.
doi:10.1371/journal.pone.0020589.t003

Discussion

1. Samples

We recruited 9 offspring from first-cousin marriages (SCZ) and 92 from non-consanguineous marriages (non-CJ). As shown in Figure 2, our non-CJ dataset and publicly available HapMap3 JPT datasets showed a common cluster, except for the presence of 3 outliers that have been reported to be potentially from consanguineous families [14,15]. This concordance suggests that our experimental quality and data processing approaches were appropriate. In this study, we analyzed a limited number of samples; however, homozygosity mapping was a reasonable strategy to adopt because it requires relatively smaller number of samples than case-control studies. We did not use samples from the parents of patients in this study because these are not very informative in our strategy. On the other hand, affected and unaffected siblings in single families are strongly informative in homozygosity mapping, and we are continuously recruiting additional siblings for future study.

2. ROH analysis

Most of the previous homozygosity mapping studies were based on genotypes derived from microsatellites or simple tandem-repeat polymorphisms (STRP). The highly polymorphic nature of multi-allelic STRP markers is suitable to cover the whole genome with a fewer numbers of markers. However, recent DNA microarray technologies have enabled massive genome-wide SNP genotyping to be performed in a short time. The problem with homozygosity mapping based on SNPs is the accurate detection of regions with ROHs. As SNPs have a less informative biallelic nature, using the naïve definition of an ROH as just a contiguous homozygous region may skew the detection of ROHs because of the frequency of low minor allele SNPs, genotyping errors, and "no-call" SNPs.

The solution to this problem using the Affymetrix Human Genotyping 500K arrays and Illumina Infinium HumanHap300v2 arrays was the application of ROH detection bins sliding through each chromosome to filter out low SNP density bins and to allow the small number of heterozygous SNPs and no-call SNPs to be placed in a bin [6,17]. An alternative method to detect ROHs is to adopt an HMM. Partek GS software implements the HMM-based "LOH detection" algorithm. A similar algorithm is also implemented in the Affymetrix GeneChip Chromosome Copy Number Analysis Tool (CNAT), as described in the CNAT user guide [18]. The HMM-based algorithm of these tools takes not only the information of adjacent SNP genotypes but also the heterozygosity of SNPs as a reference baseline calculated from the genotyping results in the reference samples or the *a priori* default frequency. This method is expected to more accurately detect ROH regions that reflect actual recombination.

Selection of the reference population for the baseline data is crucial for the HMM-based detection of ROHs. If the reference population is carefully selected to match the background of the case population, the baseline generated from the observation of actual SNPs in the reference population can omit ROHs resulting from LD and regions with low SNP density, such as centromeres. However, if strict matching of the used population background is difficult, use of the fixed default heterozygous frequency, whose

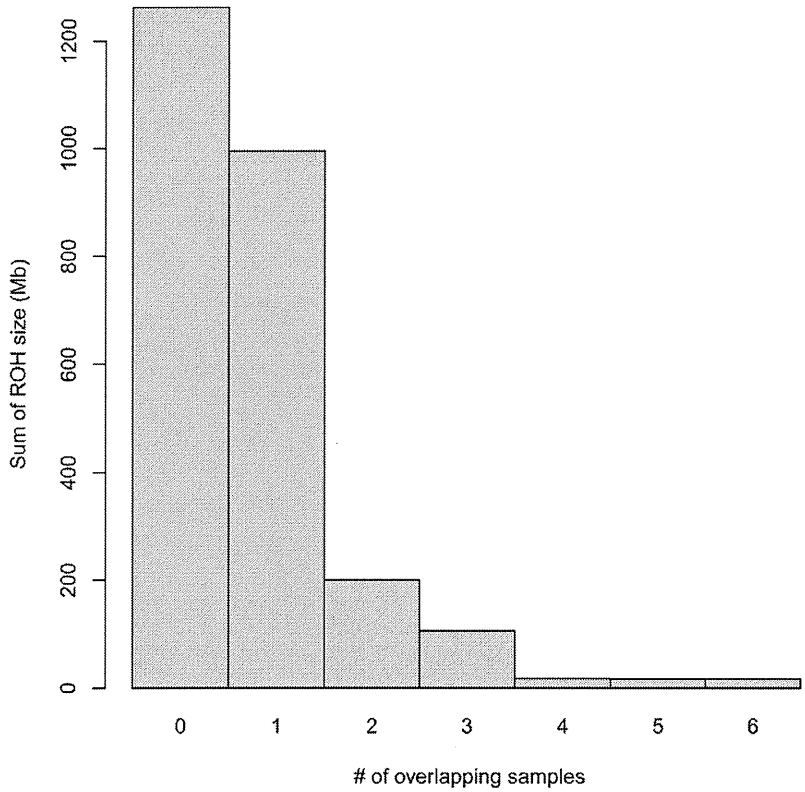

Figure 4. Sum of run of homozygosity (ROH) lengths and number of overlapping patients, excluding patient siblings. Y-axis indicates the sum of ROH lengths shared by a given number of patients. The zero column indicates the sum of ROHs not shared by any of the samples.
doi:10.1371/journal.pone.0020589.g004

default value is 0.3, still has the advantage of minimizing false-negatives in the detection of ROHs.

To determine the optimal length threshold of ROHs to extract autozygous segments from whole ROHs, we adopted OR = 3 for the analysis. This approach may work well when a large enough reference sample is available. When a reference population is not available, a threshold where the sum of the ROH length in the upper tail of its distribution is equal to the theoretical autozygous length of a genome, that is, 1/16 of a genome in the offspring of a first-cousin marriage, could be another option. In our SCZ dataset, the threshold using this approach was approximately 10.6 Mb.

Our results demonstrated obvious differences in the proportion of the length distribution of ROHs between the non-CJ and SCZ datasets. A recent report on European populations, including endogamy subpopulations, has shown that a higher proportion of individuals in endogamy subpopulations have ROHs longer than 1.5 Mb compared with other subpopulations [6]. Our scatter plot of the individual total number and size of ROHs (Figure 2) is not fully in agreement with this previous report, although the non-CJ dataset made a cluster and showed a positive correlation (Pearson product-moment correlation coefficient r = 0.773), and the SCZ dataset was scattered and showed a weak positive correlation (r = 0.432). This may be explained by the fact that the previous report excluded ROHs <500 kb to ignore ROHs that potentially resulted from LD and removed hemizygous deletions of ROHs. In this study, we did not adopt a strategy to filter ROHs by their size before the analyses because the discrimination of autozygous regions and LD simply by size is essentially impossible. Adopting a baseline file derived from a strictly matched population in the HMM-based detection of ROHs can be used instead. Additionally, differences in genotyping platforms with different SNP densities may affect the size distribution of ROHs. Although our data from the sparser Affymetrix Genotyping 10k SNP panel produced a similar bell curve-like ROH size distribution, the whole curve was shifted to the right (data not shown).

The size distribution of ROHs for a given population is affected by its inbreeding coefficient (F). Studies of consanguineous marriages in subpopulations from Japan during the 1980s compared the F values for Japan (F = 0.00134) to those in Kuwait (F = 0.0219), India (F = 0.02313), England (F = 0.00017), and the United States (F = 0.00003) [19,20]. These reports have also shown that despite the decrease in consanguineous marriages in Japan, local subpopulations have higher F-values. The same tendency has also been shown by a genealogical study that estimated inbreeding rates in large and semi-isolated populations on the basis of historical changes in population size [21]. Recently, the importance of studying endogamous populations has been stressed [22]; however, populations with intermediate F-values have advantages for our homozygosity mapping approach. This approach uses the differences in the size distribution of ROHs in a case population consisting of offspring from consanguineous marriages and a control population consisting of offspring from non-consanguineous marriages. A high F-value population may not have clear distribution differences between cases and controls. On the other hand, finding a sufficient number of cases in low F-value populations may not be easy. From this standpoint, an intermediate F-value population, such as the Japanese population,


A
1
2
3
4
5
6
7
8
9
10
11
12
13
14
15
16
17
18
19
20
21
22
B
1
2
3
4
5
6
7
8
9
10
11
12
13
14
15
16
17
18
19
20
21
22

Figure 5. Overlapping autosomal runs of homozygosity. Each autosome is shown horizontally with the number of overlapping samples (upper) and chromosome ideograms (lower). Centromeres are shown by hatched boxes. A, overlapping segments shared among 1 (isolated) to 7 samples in a total of 9 patient samples. B, overlapping segments shared by 2 patient siblings (h-I and h-II) and an additional 1–4 patient samples.
doi:10.1371/journal.pone.0020589.g005

represents an interesting dataset for our homozygosity mapping approach, as was shown previously in the Costa Rican population [23,24].

We presented here some threshold lengths of ROHs to detect IBD regions from great-grandparents. As recombination will, of course, occur everywhere by chance, small autozygous regions could be overlooked with the threshold shown here. However, no systematic analyses have so far identified IBD regions in consanguineous marriages by whole-genome SNP typing. Our method shown here, which 1) detects longer ROHs in each individual and 2) aligns ROHs and identifies overlapping regions, will be helpful for autosomal recessive disorders and also for complex disorders resulting from rare variants. If collecting patients in geographically and historically isolated areas is possible, this homozygosity mapping approach is likely to be successful. Nonetheless, the effectiveness of homozygosity mapping for complex disorders remains controversial [4]. We believe that we can uncover new candidate loci through the application of whole-genome SNP typing to homozygosity mapping because of its high density genomic coverage and high-throughput ability.

3. Possible novel loci for schizophrenia

We identified several putative SCZ loci that are presented in Figure 5 and Tables S1 and 3. In our study, we assumed the 2 models outlined in the Methods section. Model I was designed to find shared causal loci among unrelated individuals. For the other model, we hypothesized that the siblings shared the same causal loci; thus, Model II was designed to find the common loci between the siblings and unrelated individuals.

For Model I (Table S1), from the analysis of 7 unrelated individuals, the loci included the 5q23.3–q31.1 region that was previously identified by linkage analysis in the Irish population [16]. Among the genes that mapped to 5q23.3–q31.1, *HINT1* [25,26] and *ACSL6* [27] were previously reported to be possibly associated with SCZ. In patients from consanguineous families we analyzed, homozygous genomic variations may be causative for the disease (Figure 5 and Tables S1 and 3). However, small sample size in our study may be a limiting factor to generalize such conclusions. In common diseases such as psychiatric disorders, including SCZ and bipolar disorders, especially in familial cases or in cases from relatively isolated areas, rare variants possibly contribute more than common variants to the disease phenotype [28–30].

On the basis of the rare variant-common disease hypothesis, it is appropriate that the genetic etiology between sibling cases and other unrelated cases may be various. In addition, our results suggested that multiple loci influenced the susceptibility to SCZ, as other reports have suggested [31].

We presented here the systematic analyses of the homozygosity mapping method using whole genome SNP typing, and we identified ROHs that potentially contain SCZ causative recessive regions that are shared among our samples. When we explain SCZ as a result of the homozygous state of rare variant mutations, the number of overlapping individuals may be challenging, as it is possible that each individual has a different variation. The heterogeneity of SCZ may explain the lack of overlap for our results with previously reported regions [32,33]; moreover, our methodology has a limitation for detecting causative genes that are included in shorter ROHs by chance. We have shown that the Affymetrix Genome-Wide Human SNP Array 5.0 or 6.0 could be applied to special cases including first-cousin marriages to identify genomic variations. Increasing number of samples obtained from patients from consanguineous families with SCZ is important to make our results more meaningful. Furthermore, we plan to analyze genetic variants in updated ROHs by the next-generation sequencing technologies.

Supporting Information

Table S1 Novel loci identified in this study.
(DOC)

Acknowledgments

We thank Dr. Haruko Ichinose from Eijinkai Ariake Hoyouin Hospital and Drs. Takehito Sakai and Sumihisa Honda from Nagasaki University for their assistance. We also thank Dr. Pawel Stankiewicz from Baylor College of Medicine for a critical review of the manuscript.

Author Contributions

Conceived and designed the experiments: NK KI-Y HO. Performed the experiments: NK ST HM. Analyzed the data: SO AI TK NN KT. Contributed reagents/materials/analysis tools: SO AI TK NN KT. Wrote the paper: NK KI-Y HO.

References

1. Burmeister M, McInnis MG, Zöllner S (2008) Psychiatric genetics: progress amid controversy. Nat Rev Genet 9: 527–540.
2. Morrow EM, Yoo SY, Flavell SW, Kim TK, Lin Y, et al. (2008) Identifying autism loci and genes by tracing recent shared ancestry. Science 321: 218–223.
3. Bulayeva KB (2006) Overview of genetic-epidemiological studies in ethnically and demographically diverse isolates of Dagestan, Northern Caucasus, Russia. Croat Med J 47: 641–648.
4. Rudan I, Campbell H, Carothers AD, Hastie ND, Wright AF (2006) Contribution of consanguinuity to polygenic and multifactorial diseases. Nat Genet 38: 1224–1225.
5. Mansour H, Fathi W, Klei L, Wood J, Chowdari K, et al. (2010) Consanguinity and increased risk for schizophrenia in Egypt. Schizophr Res 120: 108–112.
6. McQuillan R, Leutenegger AL, Abdel-Rahman R, Franklin CS, Pericic M, et al. (2008) Runs of homozygosity in European populations. Am J Hum Genet 83: 359–372.
7. The International HapMap Consortium (2003) The International HapMap Project. Nature 426: 789–796.
8. Hong H, Su Z, Ge W, Shi L, Perkins R, et al. (2008) Assessing batch effects of genotype calling algorithm BRLMM for the Affymetrix GeneChip Human Mapping 500 K array set using 270 HapMap samples. BMC Bioinformatics 9: S17.
9. BRLMM-P: a Genotype Calling Method for the SNP 5.0 Array. Available: http://www.affymetrix.com/support/technical/whitepapers/brlmmp_whitepaper.pdf. Accessed 14 Mar 2011.
10. R Development Core Team () R: A Language and Environment for Statistical Computing. R Foundation for Statistical Computing, Vienna, Austria (2006). Available: http://www.R-project.org/. Accessed 14 Mar 2011.
11. Wand MP, Johnes MC (1995) Kernel Smoothing. Chapman and Hall, London.
12. Korn JM, Kuruvilla FG, McCarroll SA, Wysoker A, Nemesh J, et al. (2008) Integrated genotype calling and association analysis of SNPs, common copy number polymorphisms and rare CNVs. Nat Genet 40: 1253–1260.
13. The International HapMap Consortium (2005) A haplotype map of the human genome. Nature 437: 1299–1320.
14. Yang H, Chang L, Huggins RM, Chen C, Mullighan CG (2011) LOHAS: loss-of-heterozygosity analysis suite. Genet Epidemiol. In press.

15. USCS Genome Bioinformatics, Golden Path Statistics, NCBI Build 36.1 assembly, March 2006 (hg 18). Available: http://genome.ucsc.edu/goldenPath/stats.html#hg18. Accessed 14 Mar 2011.
16. Straub RE, MacLean CJ, Ma Y, Webb BT, Myakishev MV, et al. (2002) Genome-wide scans of three independent sets of 90 Irish multiplex schizophrenia families and follow-up of selected regions in all families provides evidence for multiple susceptibility genes. Mol Psychiatry 7: 542–559.
17. Lencz T, Lambert C, DeRosse P, Burdick KE, Morgan TV, et al. (2007) Runs of homozygosity reveal highly penetrant recessive loci in schizophrenia. Proc Natl Acad Sci U S A 104: 19942–19947.
18. Affymetrix GeneChip Chromosome Copy Number Analysis Tool (CNAT) Version 4.0 User Guide (2007) Affymetrix Inc.
19. Imaizumi Y (1986) A recent survey of consanguineous marriages in Japan. Clin Genet 30: 230–233.
20. Al-Awadi SA, Moussa MA, Naguib KK, Farag TI, Teebi AS, et al. (1985) Consanguinity among the Kuwaiti population. Clin Genet 27: 483–486.
21. Pattison JE (2004) A comparison of inbreeding rates in India, Japan, Europe and China. Homo 55: 113–128.
22. Editorial (2006) The germinating seed of Arab genomics. Nat Genet 38: 851.
23. McInnes LA, Service SK, Reus VI, Barnes G, Charlat O, et al. (2001) Fine-scale mapping of a locus for severe bipolar mood disorder on chromosome 18p11.3 in the Costa Rican population. Proc Natl Acad Sci U S A 98: 11485–11490.
24. Mathews CA, Reus VI, Bejarano J, Escamilla MA, Fournier E, et al. (2004) Genetic studies of neuropsychiatric disorders in Costa Rica: a model for the use of isolated populations. Psychiatr Genet 14: 13–23.
25. Chen Q, Wang X, O'Neill FA, Walsh D, Kendler KS, et al. (2008) Is the histidine triad nucleotide-binding protein 1 (HINT1) gene a candidate for schizophrenia? Schizophr Res 106: 200–207.
26. Chen X, Wang X, Hossain S, O'Neill FA, Walsh D, et al. (2006) Haplotypes spanning SPEC2, PDZ-GEF2 and ACSL6 genes are associated with schizophrenia. Hum Mol Genet 15: 3329–3342.
27. Luo XJ, Diao HB, Wang JK, Zhang H, Zhao ZM, et al. (2008) Association of haplotypes spanning PDZ-GEF2, LOC728637 and ACSL6 with schizophrenia in Han Chinese. J Med Genet 45: 818–826.
28. O'Donovan MC, Craddock NJ, Owen MJ (2009) Genetics of psychosis; insights from views across the genome. Hum Genet 126: 3–12.
29. Schork NJ, Murray SS, Frazer KA, Topol EJ (2009) Common vs. rare allele hypotheses for complex diseases. Curr Opin Genet Dev 19: 212–219.
30. Gorlov I, Gorlova O, Frazier M, Spitz M, Amos C (2011) Evolutionary evidence of the effect of rare variants on disease etiology. Clin Genet 79: 199–206.
31. Ioannidis JPA, Ntzani EE, Trikalinos TA, Contopoulos-Ioannidis DG (2001) Replication validity of genetic association studies. Nat Genet 29: 306–309.
32. Girard SL, Xiong L, Dion PA, Rouleau GA (2011) Where are the missing pieces of the schizophrenia genetics puzzle? Curr Opin Genet Dev. In press.
33. Glessner JT, Hakonarson H (2009) Common variants in polygenic schizophrenia. Genome Biol 10: 236.

Proteasome assembly defect due to a proteasome subunit beta type 8 (PSMB8) mutation causes the autoinflammatory disorder, Nakajo-Nishimura syndrome

Kazuhiko Arima[a,1], Akira Kinoshita[b,1], Hiroyuki Mishima[b,1], Nobuo Kanazawa[c,1], Takeumi Kaneko[d], Tsunehiro Mizushima[e], Kunihiro Ichinose[a], Hideki Nakamura[a], Akira Tsujino[f], Atsushi Kawakami[a], Masahiro Matsunaka[c], Shimpei Kasagi[g], Seiji Kawano[g], Shunichi Kumagai[g], Koichiro Ohmura[h], Tsuneyo Mimori[h], Makito Hirano[i], Satoshi Ueno[i], Keiko Tanaka[j], Masami Tanaka[k], Itaru Toyoshima[l], Hirotoshi Sugino[m], Akio Yamakawa[n], Keiji Tanaka[o], Norio Niikawa[p], Fukumi Furukawa[c], Shigeo Murata[d], Katsumi Eguchi[a], Hiroaki Ida[a,q,2], and Koh-ichiro Yoshiura[b,2]

[a]Unit of Translational Medicine, Department of Immunology and Rheumatology, Graduate School of Biomedical Sciences, Nagasaki University, Nagasaki 852-8501, Japan; [b]Department of Human Genetics, Graduate School of Biomedical Sciences, Nagasaki University, Nagasaki 852-8523, Japan; [c]Department of Dermatology, Wakayama Medical University, Wakayama 641-0012, Japan; [d]Laboratory of Protein Metabolism, Graduate School of Pharmaceutical Sciences, The University of Tokyo, Bunkyo-ku, Tokyo 113-0033, Japan; [e]Department of Life Science, Picobiology Institute, Graduate School of Life Science, University of Hyogo, Kamigori-cho, Ako-gun, Hyogo 678-1297, Japan; [f]Unit of Translational Medicine, Department of Neuroscience and Neurology, Nagasaki University Graduate School of Biomedical Sciences, Nagasaki 852-8501; [g]Department of Clinical Pathology and Immunology, Kobe University Graduate School of Medicine, Kobe 650-0017, Japan; [h]Department of Rheumatology and Clinical Immunology, Graduate School of Medicine, Kyoto University, Kyoto 606-8507, Japan; [i]Department of Neurology, Nara Medical University, Kashihara, Nara 634-8522, Japan; [j]Department of Neurology, Kanazawa Medical University, Kahoku-gun, Ishikawa 920-0293, Japan; [k]Department of Neurology, Utano National Hospital, Ukyou-ku, Kyoto 616-8255, Japan; [l]Department of Neurology and Medical Education Center, Akita University School of Medicine, Akita 010-8543, Japan; [m]Sugino Pediatric Clinic, Asakita-ku, Hiroshima 731-0231, Japan; [n]Office of Strategic Management, Institute of Medical Science, The University of Tokyo, Minato-ku, Tokyo 108-8639, Japan; [o]Laboratory of Protein Metabolism, Tokyo Metropolitan Institute of Medical Science, Setagaya-ku, Tokyo 156-8506, Japan; [p]Research Institute of Personalized Health Sciences, Health Sciences University of Hokkaido, Ishikari-Tobetsu, Hokkaido 061-0293, Japan; and [q]Division of Respirology, Neurology, and Rheumatology, Department of Medicine, Kurume University School of Medicine, Kurume, Fukuoka 830-0011, Japan

Edited* by Daniel Kastner, National Institutes of Health, Bethesda, MD, and approved July 21, 2011 (received for review April 14, 2011)

Nakajo-Nishimura syndrome (NNS) is a disorder that segregates in an autosomal recessive fashion. Symptoms include periodic fever, skin rash, partial lipomuscular atrophy, and joint contracture. Here, we report a mutation in the human proteasome subunit beta type 8 gene (PSMB8) that encodes the immunoproteasome subunit β5i in patients with NNS. This G201V mutation disrupts the β-sheet structure, protrudes from the loop that interfaces with the β4 subunit, and is in close proximity to the catalytic threonine residue. The β5i mutant is not efficiently incorporated during immunoproteasome biogenesis, resulting in reduced proteasome activity and accumulation of ubiquitinated and oxidized proteins within cells expressing immunoproteasomes. As a result, the level of interleukin (IL)-6 and IFN-γ inducible protein (IP)-10 in patient sera is markedly increased. Nuclear phosphorylated p38 and the secretion of IL-6 are increased in patient cells both in vitro and in vivo, which may account for the inflammatory response and periodic fever observed in these patients. These results show that a mutation within a proteasome subunit is the direct cause of a human disease and suggest that decreased proteasome activity can cause inflammation.

Nakajo-Nishimura syndrome (NNS) (MIM256040, ORPHA-2615) is a distinct inflammatory and wasting disease. It was first reported by Nakajo in 1939, followed by Nishimura in 1950, and was called "secondary hypertrophic osteoperiostosis with pernio" (1, 2). More than 20 cases of this disease have been reported in various clinical fields, all from Japan (3–8). The disease was soon recognized as a new entity and was called "a syndrome with nodular erythema, elongated and thickened fingers, and emaciation" or "hereditary lipomuscular atrophy with joint contracture, skin eruptions and hyper-γ-globulinemia" on the basis of the common characteristic features (3, 4).

NNS usually begins in early infancy with a pernio-like rash. The patient develops periodic high fever, nodular erythema-like eruptions, and myositis. Lipomuscular atrophy and joint contractures gradually progress, mainly in the upper body, to form the characteristic thin facial appearance and elongated clubbed fingers. Inflammatory changes are marked and include constantly elevated erythrocyte sedimentation rate (ESR) and C-reactive protein (CRP), hyper-γ-globulinemia, hepatosplenomegaly, basal ganglia calcification, and focal mononuclear cell infiltration with vasculopathy on histopathology. Autoantibodies are negative at the onset of NNS; although, in some cases, titers increase as the disease progresses.

Although NNS bears similarities to other autoimmune diseases, particularly dermatomyositis, it is only in recent years that its similarity to autoinflammatory periodic fever syndromes has been pointed out (5, 6). Oral steroids are effective in treating the inflammation, but not the wasting, and most patients die as a result of respiratory or cardiac failure. Despite the predicted segregation in an autosomal recessive fashion, the gene responsible has not been identified. Here, we describe a mutation in the human *PSMB8* that encodes the immunoproteasome subunit β5i in NNS patients.

Proteasomes collaborate with the ubiquitin system, which tags proteins with a polyubiquitin chain and marks them for degradation. The 26S proteasome is a multisubunit protease responsible for regulating proteolysis in eukaryotic cells in collaboration with the ubiquitin system. This ubiquitin–proteasome system is involved in various biological processes, including immune responses, DNA repair, cell cycle progression, transcription and protein quality control. It comprises a single catalytic 20S proteasome with 19S regulatory particles (RPs) attached to the ends (9–11). The 20S proteasome comprises 28 subunits arranged as a cylindrical particle containing four heteroheptameric rings: $\alpha_{1-7}\beta_{1-7}\beta_{1-7}\alpha_{1-7}$. Only three of the β subunits, β1, β2, and β5, are proteolytically active in the standard 20S pro-

Author contributions: N.K., A.Y., N.N., F.F., S.M., K.E., H.I., and K.-i.Y. designed research; K.A., A. Kinoshita, H.M., N.K., T.K., T. Mizushima, K.I., H.N., A.T., A. Kawakami, M.M., S. Kasagi, S. Kawano, S. Kumagai, K.O., T. Mimori, M.H., S.U., Keiko Tanaka, M.T., I.T., H.S., S.M., H.I., and K.-i.Y. performed research; K.A., A. Kinoshita, H.M., N.K., A.Y., S.M., H.I., and K.-i.Y. analyzed data; and N.K., Keiji Tanaka, F.F., S.M., H.I., and K.-i.Y. wrote the paper.

The authors declare no conflict of interest.

*This Direct Submission article had a prearranged editor.

[1]K.A., A. Kinoshita, H.M., and N.K. contributed equally to this work.

[2]To whom correspondence may be addressed. E-mail: kyoshi@nagasaki-u.ac.jp or ida@med.kurume-u.ac.jp.

This article contains supporting information online at www.pnas.org/lookup/suppl/doi:10.1073/pnas.1106015108/-/DCSupplemental.

teasome. Each of the three β subunits preferentially cleaves an acidic, basic, or hydrophobic residue, activities often referred to as caspase-like, trypsin-like, or chymotrypsin-like, respectively.

In vertebrates, there are three additional IFN-γ–induced subunits: β1i, β2i, and β5i. These are preferentially incorporated into the 20S proteasome in place of the standard subunits to form the immunoproteasome in immune cells such as macrophages, T and B cells, and dendritic cells, whereas their expression is low in nonlymphoid peripheral tissues. This results in more efficient production of MHC class I epitopes (12). The present study analyzed the activity of proteasomes with a mutated β5i subunit, and the subsequent inflammatory signal transduction pathways in mutant cells. The results suggest that the *PSMB8* mutation evokes an inflammatory response in humans, and that the p38 pathway may play an important role in inflammation in NNS patients.

Recently, a different mutation in the *PSMB8* gene was reported in patients with a disease similar to, but distinct from, NNS: an autosomal recessive syndrome of joint contracture, muscular atrophy, microcytic anemia, and panniculitis-associated lipodystrophy (JMP) (13, 14). The mutation in JMP syndrome, T75M, causes a reduction in chymotrypsin-like activity only, without disrupting the activity of other peptidases (13). In contrast, the G201V mutation identified in NNS patients results in the loss of all peptidase activity because of assembly defects and reduced proteasome levels. Thus, the discovery of *PSMB8* mutations in these related diseases indicates the presence of a distinct class of proteasome-associated autoinflammatory disorders.

Results

Clinical Features of NNS Patients. National surveillance in Japan confirms that only around 10 NNS patients are alive today. Therefore, preserved fibroblasts from an autopsy case (patient 1) were provided for genetic analysis, following approval by the local ethical committee. Of the living cases, written informed consent to undertake genetic and molecular analyses was obtained from six patients. The clinical features of all seven cases are summarized in Table S1. Patients 1, 2, and 4 were born to consanguineous parents and their clinical features have been described previously (Fig. S1*A*) (6, 8). The other patients are sporadic cases collected for this study and were born in the limited area between south Osaka and Wakayama. A diagnosis of NNS is not difficult owing to the characteristic features, including the thin facial appearance and long clubbed fingers (Fig. S1*B*). The clinical course throughout childhood was variable: from no medical consultation in the case of patient 7, to administration of oral steroids since infancy in patients 3 and 6. Partial lipomuscular atrophy with long clubbed fingers plus a pernio-like, heliotrope-like, or nodular erythema-like skin rash were observed in all cases, and periodic fever and joint contractures in most but not all. Wheras hyperhidrosis was also observed in some cases, short stature and low IQ were seen only in patients 6 and 1, respectively. Indeed, patient 6 was treated with growth hormone, although growth retardation in this case may have been due, in part, to oral steroids. Chronic inflammation, indicated by elevated ESR and hyper-γ-globulinemia, were observed in all patients, and microcytic anemia, high serum creatine phosphokinase (CPK), hepatosplenomegaly, and basal ganglia calcification were present in most, but not all. Notably, various autoantibodies (with a mildly elevated titer of antinuclear antibodies) were detected in half of the patients. The most striking differences between NNS and JMP are the absence of fever in JMP syndrome and the absence of seizures in NNS (14) (Table S1).

Genetic Mapping and Mutation Searches. We examined genomic DNA samples from five patients (patients 1–5) and three unaffected siblings of patient 4 using an Affymetrix GeneChip Human Mapping 500K array set (Nsp I and Sty I arrays), and the BRLMM genotyping algorithm. Because the runs of homozygosity (ROHs) shared by all patients were expected to be candidate regions containing the gene responsible for the disease, we identified a region spanning 1.1 Mb on chromosome 6p21.31–32 [from 32,798,004–33,903,106; National Center for Biotechnology Information (NCBI) build 36.1] as the sole candidate region responsible for NNS (Fig. 1*A*). We directly sequenced 436 coding exons in the 44 genes within this candidate region, including the splicing sites. A single nonsynonymous variation (not registered in the dbSNP database) was identified in exon 5 of *PSMB8* (NM_148919 in the NCBI database), designated *LMP7* or *RING10*, which encodes the LMP7 protein (β5i subunit) of the immunoproteasome. This mutation was a guanine to thymine transversion at nucleotide position 602 (c.602G > T) (Fig. 1*B*). Haplotype analysis indicated that the G201V mutation was probably introduced into the Japanese population by a single founder, as the haplotype around this mutation was identified in all patients (Fig. S1*C*). Gly201, which is a highly conserved residue in the β5i subunit (Fig. 1*C*) and among mature proteasome subunits in vertebrates (Fig. S1*D*), is substituted by Val (G201V) (Fig. 1*B*).

Impaired Immunoproteasome Assembly and Peptidase Activity. In silico modeling of the mutant β5i ($\beta5i^{G201V}$) subunit was used to infer the conformational impact of this mutation because the assembly of the proteasome is a highly orchestrated and complex process (9, 15). The β5i subunit is cleaved between amino acid residues Gly72 and Thr73 to yield the active form (16), in which the catalytic center is generated by Thr73, Asp89, Arg91, and Lys105. The mutated residue at position 201 was located at the edge of the S8 β-sheet of β5i and was close to its catalytic threonine residue Thr73 (Fig. 2*A*). The G201V substitution caused conformational changes not only in Thr73 but also in Lys105 within the catalytic center (Fig. S2). The mutation resulted in further conformational changes in the S8–H3 loop located at the

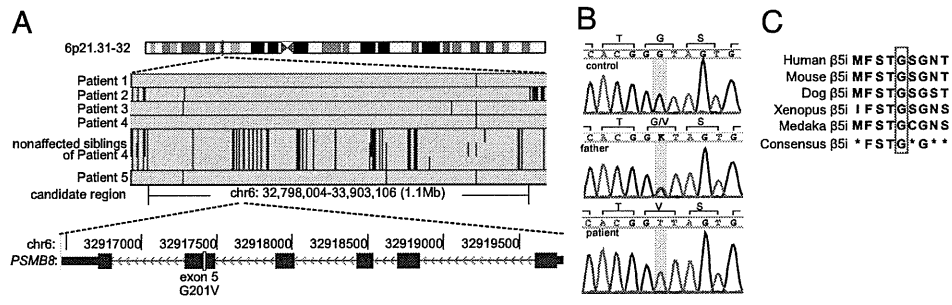

Fig. 1. SNP microarray-based homozygosity mapping and mutation search. (*A*) Homozygosity mapping for NNS patients and nonaffected siblings. ROH regions were detected using a hidden Markov model-based algorithm. The sole candidate region identified within 6p21.31–32 is shown. Green vertical lines indicate heterozygous SNPs and the background gray area indicates a region without heterozygous SNP calls. To be conservative, we did not regard isolated single heterozygous calls as delimiting ROH regions. The physical positions are shown in NCBI build 36.1. Patient numbers correspond to Figs. S1*A* and S1*C* and Table S1. No history of consanguineous marriage was apparent for patients 3 and 5, according to the family history interview. (*B*) Chromatograms for a control, a patient's father, and a patient. A mutation in *PSMB8* exon 5 identified in NNS patients by sequencing is highlighted in yellow. (*C*) Amino acid comparisons with other species. The glycine at the mutation site (red box) is highly conserved among vertebrates.

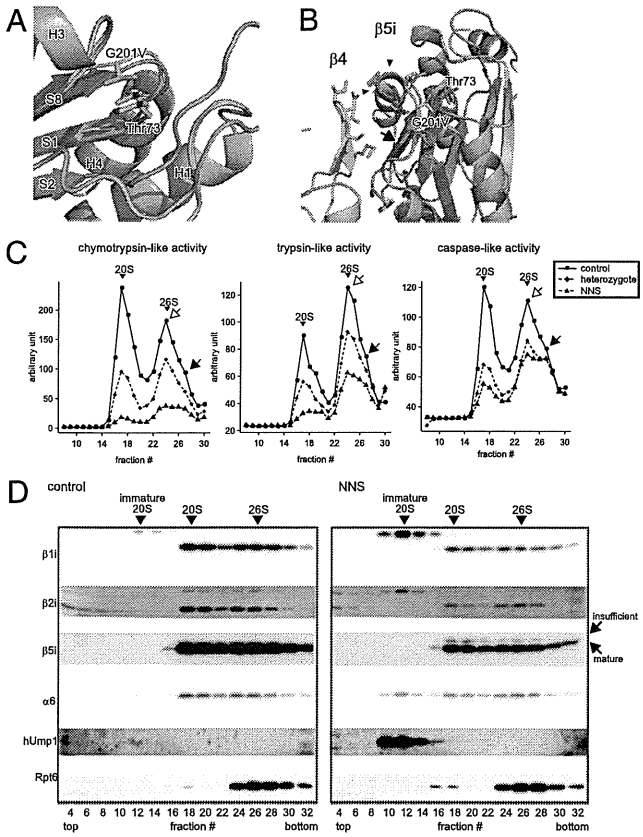

Fig. 2. G201V mutation in β5i reduces proteasome activity in immunoproteasome-expressing cells. (*A*) Close-up view of the mutation site (G201V) within β5i. Structural models of G201V β5i (orange) and wild-type β5i (green) were created from the β5-subunit structure [Protein Data Bank (PDB) ID code 1IRU]. The secondary structure elements for β5i are labeled. Val201 and Thr73 are shown in the stick model. Thr73 is a catalytic residue of β5i. (*B*) A ribbon diagram of the β4–β5i complex. The arrow shows the difference in the β-sheet between β5i (green) and $\beta5i^{G201V}$ (orange). Arrowheads show the protruding S8–H3 loop of $\beta5i^{G201V}$. (*C*) Peptidase activity of LCLs. Extracts were fractionated by glycerol gradient centrifugation (8–32% glycerol from fraction 1–32). Arrowheads indicate the peak positions of the 20S and 26S proteasomes (open arrows, single-capped 26S; closed arrows, double-capped 26S). (*D*) Western blot analysis of fractionated total LCL extracts. Western blot analysis of proteasome subunits from fractions 1–32 fractionated in C. The sedimenting positions of the immature 20S, 20S, and 26S proteasomes are indicated by arrowheads. The mature and incompletely cleaved $\beta5i^{G201V}$ subunits are indicated by arrows. The mature β5i subunit is cleaved within a C-terminal polypeptide between Gly72 and Thr73. The insufficiently cleaved β5i subunit is probably cleaved at a site toward the N terminus site, yielding a fragment with a higher molecular weight. The same amount of protein was subjected to glycerol gradient ultracentrifugation. The level of proteasome is reduced in NNS patients. Control, LCL extract from healthy control; NNS, LCL extract from patient with NNS.

interface between β4 and β5i, which affected the surface contact of β5i with the adjacent β4 subunit (Fig. 2*B*). These results suggest that the G201V mutation affects both β5i catalytic activity and assembly of the 20S proteasome.

According to Sijts and Kloetzel (17), the β1 subunit has a caspase-like function, the β2 subunit has trypsin-like activity, and the β5 subunit has chymotrypsin-like activity. Although it has not been clearly confirmed which of the immunoproteasome subunits possess which peptidase activity, it is generally thought that β5i has chymotrypsin-like activity. We next examined the influence of the β5i mutation on proteasome peptidase activity. Extracts from immortalized lymphoblastoid cell lines (LCLs) that constitutively expressed the immunoproteasome, rather than the standard proteasome, were obtained from an NNS patient, his heterozygous parent, and a healthy control, and were separated by glycerol gradient centrifugation. The fractions were then assayed for chymotrypsin-like, trypsin-like, and caspase-like activity mediated by the 20S/26S proteasomes. The results showed that not only was chymotrypsin-like activity markedly decreased in NNS cells, but the other two enzyme-like activities were also decreased (Fig. 2*C*).

Reduced Proteasome Levels. To gain further insight into the molecular mechanisms affecting peptidase activity in the mutant cells, the glycerol density gradient fractions were subjected to Western blot analysis (Fig. 2*D*). Assembly of the mammalian 20S proteasome begins with the formation of the α-ring in conjunction with a dedicated assembly chaperone, PAC1-4. The β-ring is then formed on the α-ring with the aid of another chaperone, hUmp1, resulting in the formation of half-sized immature proteasomes. The immature proteasomes then dimerize to form the 20S proteasome accompanied by cleavage of β-subunit propeptides and the degradation of hUmp1 (9). Our most noteworthy finding was the accumulation of immature 20S proteasome precursors in NNS cells before incorporation of β5i and dimerization, as indicated by the presence of the proforms of β1i and β2i, α6 and hUmp1, and the absence of β5i (Fig. 2*D*, fractions 10–14) (18). Computer modeling suggests that this assembly defect could be due to the fact that β5i, β4, and β6 line up next to each other and that the interaction between mutant $\beta5i^{G201V}$ and β4 may be disturbed (Fig. 2*B*). The reduction in peptidase activity was unlikely due to differences in the ability of 20S to associate with 19S RP, because single-capped and double-capped 26S proteasomes were detected in the glycerol fractions from an NNS patient and control LCLs (Fig. 2*C*). The assembly defect caused a reduction in the number of 20S and 26S proteasomes in NNS cells (Fig. 2*D*), which accounts for the observed decrease in activity of all three peptidases. Another intriguing observation was that a portion of the $\beta5i^{G201V}$ subunit incorporated into the mature proteasome appeared as a slower migrating band, suggesting the presence of an insufficiently cleaved form of $\beta5i^{G201V}$ (Fig. 2*D*) (16). This may have contributed to the markedly reduced chymotrypsin-like activity seen in NNS cells compared with the other two peptidase activities.

Decreased Proteolytic Activity and Accumulation of Ubiquitinated and Oxidized Proteins. To examine proteolytic activity in vitro, the ornithine decarboxylase (ODC) degradation assay was performed (19). Proteolytic activity was significantly decreased in mutant proteasomes (Fig. 3*A*). As a consequence of the altered proteasome levels and incomplete cleavage of the subunits, proteolytic activity decreased and ubiquitinated proteins accumulated in LCLs (Fig. 3*B*) and fibroblasts from NNS patients (Fig. 3*C*). In particular, there was an obvious accumulation of K48 polyubiquitinated proteins in fibroblasts (Fig. 3*C*).

Because the immunoproteasome is important for degrading oxidized proteins and defective ribosomal products (20), we examined whether such proteins accumulated in NNS cells. We found that the level of oxidized proteins increased in cultured NNS fibroblasts and after stimulation with IFN-γ (Fig. 3*D*). Taken together, these results show that the G201V substitution within β5i severely impairs assembly of the immunoproteasome, leading to decreased proteasome levels and activity in β5i-expressing cells.

We then examined whether the defect in proteasome activity was apparent in situ in NNS patients. We stained skin biopsy sections obtained from an NNS patient and used sections from a monocytic fasciitis patient as a control. CD68 is a marker for monocyte/macrophages, a cell type known to predominantly express the immunoproteasome rather than the standard proteasome (21). Inflammatory responses characterized by the infiltration of numerous $CD68^+$ cells into the skin were observed in both NNS and fasciitis samples. However, the $CD68^+$ cells in the NNS sec-

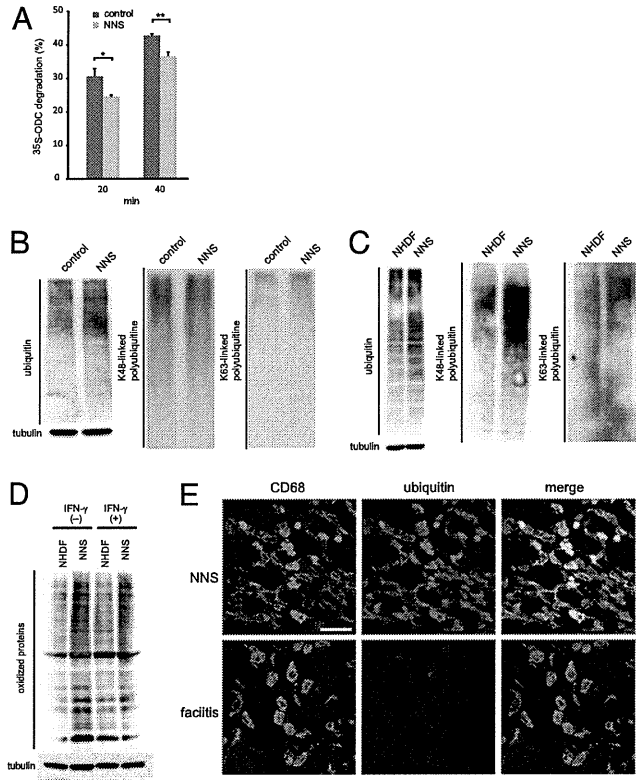

Fig. 3. Decrease of proteolytic activity and accumulation of polyubiquitinated and oxidized proteins in NNS cells. (*A*) In vitro proteolytic activity of the mutant proteasome. Degradation of recombinant ^{35}S-labeled ODC was expressed as % total ODC as described previously (11). Error bars indicated the SD of the mean ($n = 3$). $*P < 0.05$, $**P < 0.01$. (*B* and *C*) Accumulation of ubiquitinated proteins in LCLs (*B*) and fibroblasts (*C*). Western blot analysis of ubiquitinated proteins using an antiubiquitin antibody (*Left*), an anti-K48 polyubiquitinated protein antibody (*Middle*), and an anti-K63 polyubiquitinated protein antibody (*Right*). Tubulin was used as a loading control (*Lower*). NHDF, adult normal human dermal fibroblasts. (*D*) Levels of oxidized proteins determined by Oxyblot. NHDF and NNS fibroblasts were stimulated with or without 100 units of IFN-γ for 24 h. Tubulin was used as a loading control. (*E*) Immunofluorescence staining of CD68 and ubiquitinated proteins. Staining for CD68 (green) and ubiquitinated proteins (red) in skin sections from an NNS patient and a fasciitis patient. NNS ubiquitin signals showed a 4.7-fold increase with ImageJ (http://rsb.info.nih.gov/ij/) compared with fasciitis signals. (Scale bar, 10 μm.)

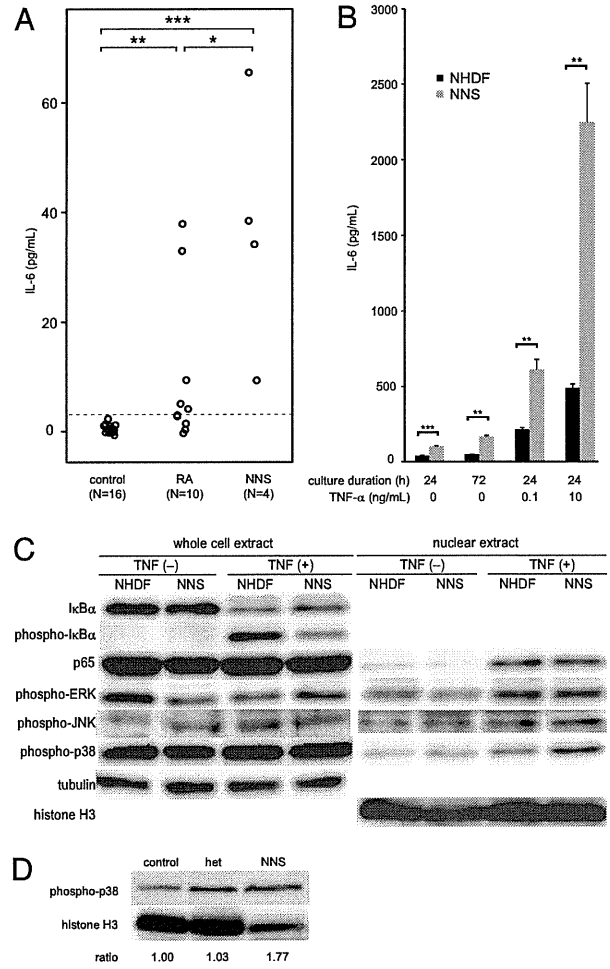

Fig. 4. Analyses of the level of IL-6 in NNS and the signal transduction system related to cytokine production. (*A*) IL-6 concentrations in sera from healthy controls, patients with NNS, and patients with rheumatoid arthritis. IL-6 levels in sera were determined by ELISA. (*B*) IL-6 production by cultured fibroblasts. The concentrations of IL-6 in conditioned media were determined by ELISA (in triplicate). (*C*) Western blot analysis for NF-κB and MAPK. Whole cell extracts and nuclear extracts were immunoblotted using antibodies against IκBα, p-IκBα, p65, p-ERK, p-JNK, and p-p38. (*D*) Western blot analysis of p-p38 in peripheral blood lymphocytes. Nuclear extracts from the peripheral blood lymphocytes of a healthy control, a heterozygous family member, and a NNS patient were blotted and visualized with anti–p-p38. Error bars indicate SD of the mean. $*P < 0.05$, $**P < 0.01$, $***P < 0.001$ [Mann-Whitney *u* test (*A*) and two-tailed Welch's *t* test (*B*)]. Signal intensities were quantified using ImageJ and expressed as fold changes relative to a healthy control normalized to histone H3 (*D*).

tions were strongly positive for ubiquitin, whereas ubiquitin was only faintly detectable in the fasciitis sections (Fig. 3*E*).

Increased IL-6 and IP-10 Levels in NNS Patient Sera and Signal Transduction in NNS Fibroblasts. We next screened NNS patient sera for inflammatory cytokines using a multiplex bead-based ELISA on a suspension array. The results showed a significant increase in the levels of interleukin (IL)-6, IFN-γ–inducible protein (IP)-10, granulocyte colony stimulating factor, and monocyte chemoattractant protein-1 (Fig. S3*A*). IL-6 was of particular interest because it is a pleiotropic cytokine with a wide range of biological activities, and it plays a key role of immune regulation, hematopoiesis, oncogenesis, and inflammation (22–24). Increased IL-6 levels in NNS sera were confirmed using a standard ELISA (Fig. 4*A*). IL-6 production was significantly higher in NNS patient fibroblasts than in healthy control fibroblasts both in the presence and absence of TNF-α (Fig. 4*B*). The serum concentration of IP-10 was also higher than that in healthy controls (Fig. S3 *A* and *B*). We measured the level of IP-10 in conditional media from cultured fibroblasts using an ELISA, but found no significant difference under the conventional culture condition, although NNS cells tended to overproduce IP-10 after stimulation with 10 ng/mL TNF-α (Fig. S3*C*).

We next investigated the various signal transduction pathways that could be responsible for IL-6 overproduction by NNS fibroblasts. Nuclear factor (NF)-κB and AP-1 are the two major transcription factors that induce proinflammatory cytokines, including IL-6 (25, 26). We used an EMSA to detect activated NF-κB in cells treated with TNF-α; however, no differences in the amount of the p65/p50 heterodimer were observed in nuclear extracts from NNS fibroblasts and healthy control fibroblasts (Fig. S4 *A* and *B*). Consistent with this result, IκBα degradation and nuclear translocation of NF-κB were not enhanced in NNS fibroblasts (Fig. 4*C*). Although activation of NF-κB is largely dependent on the ubiquitin–proteasome system, these results

suggest that decreased proteasome activity does not have much influence on the regulation of NF-κB signaling in NNS cells.

We next measured the molecules that activate AP-1, including JNK1/2/3, ERK1/2, and p38, by Western blot analysis (27, 28). The amount of phosphorylated p38 (p-p38) in the nuclear extracts from NNS fibroblasts was increased (Fig. 4*C*), irrespective of TNF-α stimulation; however, there was no obvious difference in the levels of JNK1/2/3 and ERK1/2 (Fig. 4*C*). We also observed increased levels of p-p38 in the nuclear extracts from NNS peripheral blood lymphocytes (Fig. 4*D*). The build-up of oxidized proteins and/or reactive oxygen species (ROS) within NNS fibroblasts may be one of the mechanisms responsible for the accumulation of p-p38 (29, 30).

Discussion

We have identified a point mutation in the gene encoding the immunoproteasome subunit β5i as the cause of NNS. This mutation interferes with the assembly of the 20S proteasome in cells expressing immunoproteasomes. The mutation is described as c.602G > T, and results in a Gly201 to Val (G201V) (NM_148919) substitution in the immunoproteasome β5i subunit. Although a heterozygous carrier showed reduced proteasome peptidase activity, carriers had no clinical symptoms. Thus, the NNS phenotype may be due to a reduction in total proteasome enzymatic activity below the threshold necessary for maintaining cellular homeostasis in homozygous individuals.

The *PSMB8* mutation, c.224C > T (Thr75Met), occurs in patients with JMP syndrome (13). Mutant β5i in JMP patients results in a clear reduction in chymotrypsin-like activity only, with no disruption of other peptidase activities. However, the G201V mutation we identified in NNS patients causes losses of all peptidase activity owing to assembly defects and reduced proteasome levels. The T75M mutation is probably rapidly incorporated to the proteasome complex during biogenesis and is specific for chymotrypsin-like activity. The differences between the JMP syndrome and NNS phenotypes, including cytokine production by various cells during inflammatory or noninflammatory states, need to be clarified because these differences could result from a reduction in chymotrypsin-like activity in JMP syndrome or from reductions in chymotrypsin-, trypsin-, and caspase-like activity in NNS. One of the main differences between NNS and JMP syndrome is the level of IFN-γ. IFN-γ levels are increased in JMP patients, but are within the normal range in NNS patients (Fig. S3*A*). The basis for this difference is unclear. It is possible that IFN-γ levels may not increase when all three peptidase activities are inhibited.

We also found increased IP-10 levels in patient sera using ELISA on suspension arrays. There were no significant differences in IP-10 levels between nonstimulated NNS fibroblasts and control cells, although NNS fibroblasts tended to overproduce IP-10 after stimulation with TNF-α (Fig. S3 *B* and *C*). This may reflect the proinflammatory state in NNS cells, or an increased sensitivity to cytokines (31). Because IP-10 is categorized as an inflammatory chemokine produced by various types of cells, it may play an important role in leukocyte homing to inflamed tissues and in perpetuating inflammation in various autoimmune diseases such as rheumatoid arthritis, systemic lupus erythematosus, systemic sclerosis, and multiple sclerosis (32). Thus, IP-10 may enhance inflammation in NNS patients and be associated with the autoantibody production that is occasionally observed.

A single base deletion in the 5′-UTR of hUmp1 causes keratosis linearis with ichthyosis congenita and sclerosing keratoderma (KLICK) syndrome, which is characterized by palmoplantar keratoderma (33) related to proteasome activity. This mutation results in changes in hUmp1 levels and alterations in the epidermal distribution of hUmp1 and proteasomal subunits. It is unclear how the proteasome functions in KLICK syndrome, although it is clear that disturbances in proteasome function cause clinical phenotypes in humans.

Studies in animal models indicate that cells deficient in various immunoproteasome subunits show poor CD8 responses when challenged with epitopes (34, 35) and may display alterations in the T-cell receptor (TCR) repertoire (36). In particular, β5i-deficient mice show increased susceptibility to pathogens, most likely due to the reduced efficiency of antigen presentation by β5i-deficient cells (12). Actually, in NNS patients, unresponsiveness to an intradermally applied purified protein derivative of *Mycobacterium tuberculosis* has been reported; however, there are no documented changes in susceptibility to pathogens, and no abnormalities in the number of any particular T-cell subset have been observed, apart from reduced NK activity (4). Conversely, there are no reports that β5i-deficient mice show the type of systemic inflammation observed in NNS patients.

In general, gene-deficient mice are very useful tools for analyzing the functions of target genes; however, the $\beta5i^{G201V}$ mutation shows a type of "enzymatic dominant-negative interference," which abrogates not only chymotrypsin-like activity (due to the mutation) but also the activity of the entire proteasome (due to defective assembly). Thus, it is not surprising that the phenotype seen in NNS is different from that seen in *Psmb8* knockout mice (12, 20) or after treatment with PR-957 inhibitors (37). Thus, analysis of patients with NNS and JMP syndrome and mice knocked in with these mutations would provide new insights into the function of the immunoproteasome in vivo.

Finally, we observed increased levels of p-p38 in nuclear extracts from NNS peripheral blood lymphocytes (Fig. 4*D*), although it remains unknown precisely how attenuation of proteasome activity causes accumulation of p-p38 in the nucleus. The

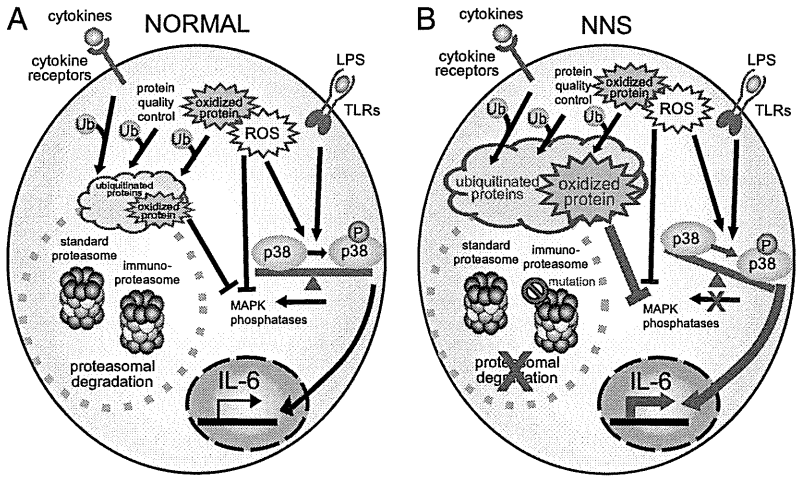

Fig. 5. Schematic model showing induction of inflammation in NNS patients with the *PSMB8* mutation. Our data are based on the scheme proposed by Bulua et al. (40). (*A*) In a normal cell, ubiquitinated or oxidized proteins generated by various stressors, including cytokines, are cleared by proteasomes. (*B*) The ubiquitinated and oxidized proteins accumulate in a cell with the *PSMB8* mutation (NNS cell). ROS and/or oxidized proteins may cause phosphorylation of p-38 to predominate over the nonphosphorylated form by inhibiting MAPK phosphatase or by activating MAPK.

accumulation of oxidized proteins and/or ROS in NNS fibroblasts may be one of the mechanisms responsible for the accumulation of p-p38 (29, 30, 38, 39). Increased p-p38 levels are in agreement with the proposed mechanism for TNFR1-associated periodic syndrome (TRAPS), which is another autoinflammatory syndrome (40).

To date, proteasome inhibitors have been used clinically to treat multiple myeloma and mantle cell lymphoma and are also effective for experimental autoimmune and inflammatory phenotypes, such as arthritis (37) and systemic lupus erythematosus (41). Generally, it is said that proteasome inhibitors induce apoptosis and inhibit immune responses. However, our results indicate that inhibiting the immunoproteasome can induce inflammatory reactions under some circumstances. In this context, the *PSMB8* mutation in NNS can be mimicked by histiocytoid Sweet syndrome (42) and cutaneous vasculitis (43) induced by bortezomib, a nonspecific proteasome inhibitor.

Taken together, the data in the present study suggest that reduction in proteasome activity affects signal transduction and promotes inflammation (Fig. 5). In NNS patients with the *PSMB8* mutation, inflammation causes ubiquitinated proteins to accumulate (compounding the effects on joints, skin, and muscle). These intracellular aggregates may then trigger innate immune responses and increased ROS production (increasing the levels of oxidized proteins), which then, through the activity of p-p38, activate the AP1 transcription factor causing an increase in the secretion of various cytokines such as IL-6.

Materials and Methods

Homozygosity Mapping. The genome-wide ROH overlap pattern was detected using in-house Ruby script (available on request) (44).

Glycerol Density Gradient Separation. Proteins from cell extracts (600 ìg) were separated into 32 fractions by centrifugation (22 h at 100,000 × *g*) in 8 -32 % (vol/vol) linear glycerol gradients.

Additional materials and methods are available in *SI Materials and Methods*.

ACKNOWLEDGMENTS. We thank the families for their participation. We also thank Prof. M. Nakashima for valuable discussion and Ms. C. Hayashida and M. Ohga for technical assistance. This work was supported, in part, by grants from the Ministry of Health, Labour, and Welfare (to F.F., N.K, and K.-i.Y.), the Japan Society for the Promotion of Science (22591094 to H.I., 21390100 to K.-i.Y., 20590331 to A. Kinoshita, 21791566 to H.M., 23791115 to K.A., and 23591651 to N.K.), the Takeda Scientific Foundation and the Naito Foundation (K.i.-Y.), and the Lydia O'Leary Memorial Foundation (N.K.).

1. Nakajo A (1939) Secondary hypertrophic osteoperiostosis with pernio. *J Dermatol Urol* 45:77–86.
2. Nishimura N, Deki T, Kato S (1950) Secondary hypertrophic osteoperiostosis with pernio-like skin lesions observed in two families. *J Dermatol Venereol* 60:136–141.
3. Kitano Y, Matsunaga E, Morimoto T, Okada N, Sano S (1985) A syndrome with nodular erythema, elongated and thickened fingers, and emaciation. *Arch Dermatol* 121: 1053–1056.
4. Tanaka M, et al. (1993) Hereditary lipo-muscular atrophy with joint contracture, skin eruptions and hyper-gamma-globulinemia: A new syndrome. *Intern Med* 32:42–45.
5. Horikoshi A, Iwabuchi S, Iizuka Y, Hagiwara T, Amaki I (1980) A case of partial lipodystrophy with erythema, dactylic deformities, calcification of the basal ganglia, immunological disorders, and low IQ level (Translated from Japanese). *Rinsho Shinkeigaku* 20:173–180.
6. Kasagi S, et al. (2008) A case of periodic-fever-syndrome-like disorder with lipodystrophy, myositis, and autoimmune abnormalities. *Mod Rheumatol* 18:203–207.
7. Oyanagi K, et al. (1987) An autopsy case of a syndrome with muscular atrophy, decreased subcutaneous fat, skin eruption and hyper gamma-globulinemia: Peculiar vascular changes and muscle fiber degeneration. *Acta Neuropathol* 73:313–319.
8. Muramatsu T, Sakamoto K (1987) Secondary hypertrophic osteoperiostosis with pernio (Nakajo). *Skin Res* 29:727–731.
9. Murata S, Yashiroda H, Tanaka K (2009) Molecular mechanisms of proteasome assembly. *Nat Rev Mol Cell Biol* 10:104–115.
10. Jung T, Catalgol B, Grune T (2009) The proteasomal system. *Mol Aspects Med* 30: 191–296.
11. Tanaka K (2009) The proteasome: Overview of structure and functions. *Proc Jpn Acad Ser B Phys Biol Sci* 85:12–36.
12. Fehling HJ, et al. (1994) MHC class I expression in mice lacking the proteasome subunit LMP-7. *Science* 265:1234–1237.
13. Agarwal AK, et al. (2010) PSMB8 encoding the β5i proteasome subunit is mutated in joint contractures, muscle atrophy, microcytic anemia, and panniculitis-induced lipodystrophy syndrome. *Am J Hum Genet* 87:866–872.
14. Garg A, et al. (2010) An autosomal recessive syndrome of joint contracture, muscular atrophy, microcytic anemia, and panniculitis-associated lipodystrophy. *J Clin Endocrinol Metab* 95:E48–E63.
15. Unno M, et al. (2002) The structure of the mammalian 20S proteasome at 2.75 A resolution. *Structure* 10:609–618.
16. Seemuller E, Lupas A, Baumeister W (1996) Autocatalytic processing of the 20S proteasome. *Nature* 382:468–471.
17. Sijts EJAM, Kloetzel P-M (2011) The role of the proteasome in the generation of MHC class I ligands and immune responses. *Cell Mol Life Sci* 68:1491–1502.
18. Hirano Y, et al. (2008) Dissecting beta-ring assembly pathway of the mammalian 20S proteasome. *EMBO J* 27:2204–2213.
19. Hirano Y, et al. (2005) A heterodimeric complex that promotes the assembly of mammalian 20S proteasomes. *Nature* 437:1381–1385.
20. Seifert U, et al. (2010) Immunoproteasomes preserve protein homeostasis upon interferon-induced oxidative stress. *Cell* 142:613–624.
21. Froment C, et al. (2005) A quantitative proteomic approach using two-dimensional gel electrophoresis and isotope-coded affinity tag labeling for studying human 20S proteasome heterogeneity. *Proteomics* 5:2351–2363.
22. Akira S, Taga T, Kishimoto T (1993) Interleukin-6 in biology and medicine. *Adv Immunol* 54:1–78.
23. Kishimoto T (2005) Interleukin-6: From basic science to medicine—40 years in immunology. *Annu Rev Immunol* 23:1–21.
24. Nishimoto N, Kishimoto T (2006) Interleukin 6: From bench to bedside. *Nat Clin Pract Rheumatol* 2:619–626.
25. Gyrd-Hansen M, Meier P (2010) IAPs: From caspase inhibitors to modulators of NF-kappaB, inflammation and cancer. *Nat Rev Cancer* 10:561–574.
26. Pasparakis M (2009) Regulation of tissue homeostasis by NF-kappaB signalling: Implications for inflammatory diseases. *Nat Rev Immunol* 9:778–788.
27. Thalhamer T, McGrath MA, Harnett MM (2008) MAPKs and their relevance to arthritis and inflammation. *Rheumatology (Oxford)* 47:409–414.
28. Kumar S, Boehm J, Lee JC (2003) p38 MAP kinases: Key signalling molecules as therapeutic targets for inflammatory diseases. *Nat Rev Drug Discov* 2:717–726.
29. Kamata H, et al. (2005) Reactive oxygen species promote TNFalpha-induced death and sustained JNK activation by inhibiting MAP kinase phosphatases. *Cell* 120: 649–661.
30. Park GB, et al. (2010) Endoplasmic reticulum stress-mediated apoptosis of EBV-transformed B cells by cross-linking of CD70 is dependent upon generation of reactive oxygen species and activation of p38 MAPK and JNK pathway. *J Immunol* 185: 7274–7284.
31. Villagomez MT, Bae SJ, Ogawa I, Takenaka M, Katayama I (2004) Tumour necrosis factor-α but not interferon-γ is the main inducer of inducible protein-10 in skin fibroblasts from patients with atopic dermatitis. *Br J Dermatol* 150:910–916.
32. Lee EY, Lee Z-H, Song YW (2009) CXCL10 and autoimmune diseases. *Autoimmun Rev* 8:379–383.
33. Dahlqvist J, et al. (2010) A single-nucleotide deletion in the POMP 5′ UTR causes a transcriptional switch and altered epidermal proteasome distribution in KLICK genodermatosis. *Am J Hum Genet* 86:596–603.
34. Caudill CM, et al. (2006) T cells lacking immunoproteasome subunits MECL-1 and LMP7 hyperproliferate in response to polyclonal mitogens. *J Immunol* 176:4075–4082.
35. Hutchinson S, et al. (2011) A dominant role for the immunoproteasome in CD8+ T cell responses to murine cytomegalovirus. *PLoS ONE* 6:e14646.
36. Basler M, Moebius J, Elenich L, Groettrup M, Monaco JJ (2006) An altered T cell repertoire in MECL-1-deficient mice. *J Immunol* 176:6665–6672.
37. Muchamuel T, et al. (2009) A selective inhibitor of the immunoproteasome subunit LMP7 blocks cytokine production and attenuates progression of experimental arthritis. *Nat Med* 15:781–787.
38. Hou N, Torii S, Saito N, Hosaka M, Takeuchi T (2008) Reactive oxygen species-mediated pancreatic beta-cell death is regulated by interactions between stress-activated protein kinases, p38 and c-Jun N-terminal kinase, and mitogen-activated protein kinase phosphatases. *Endocrinology* 149:1654–1665.
39. McCubrey JA, Lahair MM, Franklin RA (2006) Reactive oxygen species-induced activation of the MAP kinase signaling pathways. *Antioxid Redox Signal* 8:1775–1789.
40. Bulua AC, et al. (2011) Mitochondrial reactive oxygen species promote production of proinflammatory cytokines and are elevated in TNFR1-associated periodic syndrome (TRAPS). *J Exp Med* 208:519–533.
41. Neubert K, et al. (2008) The proteasome inhibitor bortezomib depletes plasma cells and protects mice with lupus-like disease from nephritis. *Nat Med* 14:748–755.
42. Murase JE, et al. (2009) Bortezomib-induced histiocytoid Sweet syndrome. *J Am Acad Dermatol* 60:496–497.
43. Gerecitano J, et al. (2006) Drug-induced cutaneous vasculitis in patients with non-Hodgkin lymphoma treated with the novel proteasome inhibitor bortezomib: A possible surrogate marker of response? *Br J Haematol* 134:391–398.
44. Kurotaki N, et al. (2011) Identification of novel schizophrenia Loci by homozygosity mapping using DNA microarray analysis. *PLoS ONE* 6:e20589.

Rheumatol Int (2012) 32:483–487
DOI 10.1007/s00296-010-1770-1

SHORT COMMUNICATION

Long-term follow-up of adalimumab monotherapy for rheumatoid arthritis in Japanese patients: a report of six cases

Kunihiro Ichinose · Tomoki Origuchi · Shin-ya Kawashiri · Naoki Iwamoto · Keita Fujikawa · Toshiyuki Aramaki · Makoto Kamachi · Kazuhiko Arima · Mami Tamai · Hideki Nakamura · Hiroaki Ida · Atsushi Kawakami · Katsumi Eguchi

Received: 1 September 2010 / Accepted: 30 December 2010 / Published online: 18 January 2011

Abstract We present six cases of patients with Japanese rheumatoid arthritis (RA) treated with a tumor necrosis factor (TNF)-alpha blocking agent, adalimumab as monotherapy for 220 weeks. All six patients were women, and the median age was 54.0 ± 7.07 years old. The median duration of the disease was 7.43 ± 11.1 years, and the median disease activity score (DAS28-CRP) was 5.35 ± 0.69. Three of six patients were able to continue to receive this treatment for 220 weeks successfully, and the DAS28-CRP decreased to 1.89 ± 0.75. Two patients withdrew because of lack of efficacy, and one patient withdrew because of adverse events (non-Hodgkin lymphoma). Adalimumab resulted in a sustained clinical response in RA patients during 220-week follow-up.

Keywords Rheumatoid arthritis (RA) · Adalimumab · Long-term · DAS28-CRP

Abbreviations

RA	Rheumatoid arthritis
DAS28-CRP	The 28 joint count Disease Activity Score using C reactive protein
CRP	C-reactive protein
TNF-α	Tumor necrosis factor alpha
ACR	American college of rheumatology
DMARD	Disease modifying anti-rheumatic drug
CHANGE	Clinical investigation in Highly disease-affected rheumatoid Arthritis patients in Japan with Adalimumab applying staNdard and General Evaluation
VAS	Visual analog scale
mHAQ	Modified health assessment questionnaire
RATIO	The French research axed on tolerance of biotherapies
ARMADA	Anti-TNF research study program of the monoclonal antibody D2E7 in rheumatoid arthritis
AAA	Anti-adalimumab antibody

Rheumatoid arthritis (RA) is a chronic inflammatory disorder characterized by progressive inflammatory synovitis and erosion of articular cartilage and marginal bone that generally begins early in the disease course [1]. Although the pathophysiology of RA is not well understood, the proinflammatory cytokine tumor necrosis factor (TNF)-α plays an important role in the pathogenesis of RA, and it is a prime target for directed biologic agents [2]. Two TNF inhibitors, infliximab [3] (75% human and 25% mouse peptide sequences, monoclonal antibody to TNF-α) and etanercept [4] (a recombinant, human, TNF receptor-Fc fusion protein), were already commercially available. The first fully human (100% human peptide sequences) therapeutic monoclonal antibody that blocks TNF-α, adalimumab (D2E7; Abbott Laboratories, Abbott Park, IL), was approved for use and has been extensively studied in clinical trials for treatment of RA [5]. To date, study authors have reported the short-term

K. Ichinose (✉) · S. Kawashiri · N. Iwamoto · K. Fujikawa · T. Aramaki · M. Kamachi · K. Arima · M. Tamai · H. Nakamura · H. Ida · A. Kawakami · K. Eguchi
Department of Rheumatology, Unit of Translational Medicine, Graduate School of Biomedical Sciences, Nagasaki University, 1-7-1 Sakamoto, Nagasaki 852-8501, Japan
e-mail: kunizo1234abcd@yahoo.co.jp

T. Origuchi
Department of Physical Therapy, Unit of Rehabilitation, Graduate School of Biomedical Sciences, Nagasaki University, Nagasaki, Japan

efficacy of adalimumab in patients with RA. In Japan, adalimumab was approved to be used for RA patients in 2007, and the efficacy and safety were reported by Miyasaka et al. [6]. However, there has been no report about the long-term efficacy of adalimumab for Japanese RA patients. The objectives of this study were to assess the sustained efficacy of adalimumab in long-term monotherapy for Japanese patients and to evaluate the long-term safety and tolerability of adalimumab given subcutaneously. This is the first report of the long-term follow-up data (220 weeks) of six RA cases treated with adalimumab monotherapy in Japan.

This study was a multicenter, open trial of adalimumab given as monotherapy performed from October 2002 through April 2008. We treated 6 patients with RA, each of whom fulfilled the 1987 revised American College of Rheumatology (ACR) criteria [7] for 3 months or more and had $\geq$12 tender joints and $\geq$10 swollen joints (excluding distal interphalangeal joints). They also had a C-reactive protein (CRP) concentration $\geq$2 mg/dl and a Disease Activity Score 28 (DAS28) $\geq$3.2, despite receiving standard anti-rheumatic treatment including at least one conventional Disease Modifying Anti-Rheumatic Drug (DMARD). Prior therapy with DMARD was discontinued at least 28 days before entry in the present study and returned for baseline visit within 42 days. The patients who were treated with biologic agents, including anti-CD4 antibody, within 6 months or prior treatment with any TNF antagonist or an alkylating agent were excluded. They gave their informed consent to the protocol, which was approved by the Institutional Review Board of Nagasaki University.

Table 1 summarizes the profiles of the 6 RA patients. None of the patients had received prior therapy with biologic agents. Patients were injected adalimumab by a physician at 20, 40, or 80 mg subcutaneously every other week for 220 weeks. Patients stopped taking current anti-rheumatic therapy, including any DMARDs, 28 days before starting this treatment. They were allowed to continue glucocorticoids (prednisolone equivalent $\leq$10 mg/day) and non-steroidal anti-inflammatory drugs, provided that the dosage regimens were stable from 28 days before starting the treatment to the end of the treatment. If the treatment was not effective, the doses of adalimumab were increased (cases 1 and 2, 20–40 mg at week 22; case 6, 40–80 mg at week 16). In case 5, the dose was decreased from 80 to 40 mg at week 22 because of the good response.

The effectiveness of adalimumab for 6 cases of RA patients was assessed at weeks 4, 16, and 28, and every 12 weeks in the extension phase using tender joint counts (TJC), swollen joint counts (SJC), visual analog scale (VAS) score, C-reactive protein (CRP), and DAS28-CRP (calculated using CRP concentration and evaluation of 28 joints) (Fig. 1). All 6 patients were women, and the median age was 54.0 $\pm$ 7.07 years old. The median duration of the disease was 7.43 $\pm$ 11.1 years, and the median score of DAS28-CRP at entry was 5.35 $\pm$ 0.69. Three patients were able to continue receiving adalimumab monotherapy for 220 weeks successfully. The median score on DAS28-CRP became 3.52 $\pm$ 1.61 at week 24, 2.79 $\pm$ 1.15 at week 48 and had decreased to 1.89 $\pm$ 0.75 by week 220. All three patients who could continue this treatment for 220 weeks showed a response for 220 weeks and achieved clinical low disease activity (DAS28-CRP <2.7).

Two patients withdrew because of lack of efficacy (case 1 discontinued at week 46; case 6 discontinued at week

Table 1 Demographic and clinical characteristics of 6 rheumatoid arthritis (RA) patients

Case	1	2	3	4	5	6	Mean $\pm$ SD
Age	53	53	52	42	58	56	54.0 $\pm$ 7.07
Sex	F	F	F	F	F	F	
BW	54.7	56	62.4	48	60.4	59.3	56.8 $\pm$ 5.16
Disease duration (years)	1.6	29.4	8	1.9	0.7	3	7.43 $\pm$ 11.1
Number of DMARDs	2	1	2	2	1	1	1.50 $\pm$ 0.55
Prednisone (mg/day)	5	5	6	5	4	4	4.83 $\pm$ 0.75
TJC	16	28	24	9	15	18	18.3 $\pm$ 6.77
SJC	10	9	17	9	13	10	11.3 $\pm$ 3.14
CRP (mg/dl)	8.02	1.25	0.38	1.63	1.21	4.96	2.91 $\pm$ 2.97
VAS (mm)	60	70	17	37	47	81	52.0 $\pm$ 23.3
mHAQ	2.25	2	1	0.5	0.5	0.875	1.19 $\pm$ 0.76
Duration of morning stiffness (min)	90	120	60	0	0	0	45.0 $\pm$ 52.8
DAS28-CRP	5.72	5.99	5.09	4.25	5.05	6.01	5.35 $\pm$ 0.69
Rheumatoid factor (IU/ml)	5	161	40	42	16	18	47.0 $\pm$ 57.7

F Female, *BW* body weight, *DMARDs* disease modifying anti-rheumatic drugs, *TJC* tender joint count, *SJC* swollen joint count, *CRP* C-reactive protein, *VAS* visual analog scale, *mHAQ* modified Health Assessment Questionnaire, *DAS28-CRP* the 28 joint count Disease Activity Score using C-reactive protein